TUBE BENDING WITH AXIAL PULL AND INTERNAL PRESSURE

A Thesis

by

ROHIT AGARWAL

Submitted to the Office of Graduate Studies of
Texas A&M University
in partial fulfillment of the requirements for the degree of

MASTER OF SCIENCE

May 2004

Major Subject: Mechanical Engineering

TUBE BENDING WITH AXIAL PULL AND INTERNAL PRESSURE

A Thesis

by

ROHIT AGARWAL

Submitted to Texas A&M University
in partial fulfillment of the requirements
for the degree of

MASTER OF SCIENCE

Approved as to style and content by:

Jyhwen Wang (Co-Chair of Committee)	Richard Alexander (Co-Chair of Committee)
Steve Suh (Member)	Dennis L. O'Neal (Interim Head of Department)

May 2004

Major Subject: Mechanical Engineering

ABSTRACT

Tube Bending with Axial Pull and Internal Pressure.

(May 2004)

Rohit Agarwal, B.E., Bangalore University, India

Co-Chairs of Advisory Committee: Dr. Jyhwen Wang
Dr. Richard Alexander

Tube bending is a widely used manufacturing process in the aerospace, automotive, and other industries. During tube bending, considerable in-plane distortion and thickness variation occurs. The thickness increases at the intrados (surface of tube in contact with the die) and it reduces at the extrados (outer surface of the tube). In some cases, when the bend die radius is small, wrinkling occurs at the intrados. In industry a mandrel is used to eliminate wrinkling and reduce distortion. However, in the case of a close bend die radius, use of a mandrel should be avoided as bending with the mandrel increases the thinning of the wall at the extrados, which is undesirable in the manufacturing operation.

The present research focuses on additional loadings such as axial force and internal pressure which can be used to achieve better shape control and thickness distribution of the tube. Based on plasticity theories, an analytical model is developed to predict cross section distortion and thickness change of tubes under various loading conditions. Results from both the FEA and analytical model indicated that at the intrados the increase in thickness for bending with internal pressure and bending with combined axial pull and internal pressure was nearly the same. But in the case of bending with the combination of axial pull and internal pressure there was a significant reduction of thickness at the extrados.

A parametric study was conducted for the case of bending with combined internal pressure and axial pull and it was seen that with proper selection of the pressure and axial pull wrinkling can be eliminated, thickness distribution around the tube can be optimized, and cross section distortion of the tube can be reduced.

Predictions of the analytical model are in good agreement with finite element simulations and published experimental results. The model can be used to evaluate tooling and process design in tube bending.

This thesis is dedicated to my Father, Mother and Brother

ACKNOWLEDGEMENTS

I would like to express the deepest appreciation to my advisor, Dr. Jyhwen Wang for providing me an opportunity to work under his guidance. With his attitude and substance of a genius: he continually and convincingly conveyed a spirit of enthusiasm, inspiration and great efforts in regard to my thesis. Without his guidance and persistent help this research would not have been possible.

The completion of this thesis would not have been possible without the support from Dr. Richard Alexander who provided important remarks and suggestions at various stages of my research. I will always be thankful to him for honing my presentation skills, which will be an asset in my future endeavors. I would also like to take this opportunity to thank Dr. Steve Suh for serving on my thesis committee and always being ready to go through any formalities.

A special thanks to Dr. Abu-Odeh Akram for his support with computer software which made a valuable contribution to my thesis. Thanks also go to the Evans library for providing clean, quiet, and well-equipped repository and database of highest order.

I would like to express my highest gratitude to my family, relatives and friends for always inspiring, supporting, and believing in all my ventures.

Finally I would like to acknowledge the services of all those who have helped me directly or indirectly from Texas A & M University to complete my research.

TABLE OF CONTENTS

CHAPTER Page

LIST OF FIGURES

FIGURE Page

FIGURE Page

LIST OF TABLES

NOMENCLATURE

r	mean radius of tube
t	initial wall thickness of tube
R	radius of bend die or center line radius
θ	bending angle or degree of bend
F	axial pull applied to the tube in the direction opposite to the tube movement
α	span angle of the tube
P_i	applied internal pressure
dP_{xm}	axial internal force induced in element due to the bending moment
A	area of cross-section of the tube
σ_{xm}	longitudinal stress induced in the tube due to the bending moment
dP_{xf}	axial force induced in element due to the applied axial force
σ_{xf}	axial stress due to the applied axial force $\sigma_{xf} = \frac{F}{2\pi rt}$
dP_x	resultant axial force acting on the element
σ_x	resultant axial stress acting on the tube
dv	centripetal force acting on the element
dP_c	circumferential force acting on the element
$d\sigma_c$	circumferential stress acting on the element
y	vertical distance of the element from the tube center
K	geometric parameter $K = \ln \frac{R + r}{(R + r\cos\alpha)}$

σ_c	circumferential stress acting on the tube
σ_r	radial stress acting on the tube
Y	yield strength of tube material
σ_{xp}	longitudinal stress induced in the tube due to internal pressure
σ_{cp}	circumferential stress or hoop stress induced in the tube due to internal pressure
σ_{xo}	resultant axial stress at extrados
σ_{co}	circumferential stress at extrados
σ_{ro}	radial stress at extrados
σ_{xi}	resultant axial stress at intrados
σ_{ci}	circumferential stress at intrados
σ_{ri}	radial stress at intrados
ε_x	longitudinal strain
ε_{xb}	longitudinal bending strain
ε_{xt}	longitudinal tensile strain
e	neutral axis shift
ϕ	neutral axis shift in degrees
ε_c	circumferential strain
ε_r	radial strain
t_α	thickness of the tube at an angle α after bending
t_{α_ext}	thickness of tube at extrados after bending

t_{α_int}	thickness of tube at intrados after bending
ε_{co}	circumferential strain at extrados
ε_{ci}	circumferential strain at intrados
r_{α}	final radius of the tube thickness of tube at extrados after bending
r_{α_ext}	radius of tube at extrados after bending
r_{α_int}	radius of tube at intrados after bending
Ω	cross section distortion
D_{max}	maximum diameter of the major axis of tube
D_{min}	minimum diameter of the minor axis of the tube
D_o	initial diameter of tube
OD	outside diameter of tube

CHAPTER I

INTRODUCTION

Tube bending processes are widely used to manufacture parts in aerospace, automotive, oil and other industries. Tubes are used as components in manufacturing of parts in numerous industries. Their application ranges from simple household items to sophisticated aerospace parts. Wherever tubes are used, accurate bend angle and uniform cross section are often desired. In the past decade, tubes have found many new applications in the automotive industry. Tube hydroforming has been identified as a new technology to manufacture parts. Tube hydroforming has many advantages in comparison with conventional manufacturing via stamping and welding. It can reduce the weight of the component, retain and even improve the strength and stiffness, reduce tooling cost due to fewer parts and tube hydroforming requires fewer secondary operations [1-3]. In most cases, the first step of tube hydroforming is bending of the tube to the required shape. The tube is bent to the approximate centerline of the final part to enable the tube to be placed in the die cavity [4]. The performance of tube hydroforming depends upon the pre-bending process. Recently Ford Motor Company used hydroforming to manufacture the chassis of its new model Ford F150.

The thesis follows the style and format of ASME Journal of Manufacturing Science and Engineering.

1.1 Tube Bending Process

There are many ways by which a tube can be bent into the required radius. The main techniques by which tube can be bent into the desired shape are rotary draw tube bending, compression tube bending, roll bending and stretch bending. The selection of technique depends upon the following factors [5]:

1. The quality of the bend and production rate desired.
2. Diameter, wall thickness and minimum bend radius desired.

1.1.1 Rotary Draw Tube Bending

Rotary draw tube bending is the most flexible bending method and is used immensely in industry on account of its tooling and low cost. The tooling consists of a bend die, clamp die, pressure die and wiper die. In this bending technique the tube is securely clamped to the bend die by using the clamp die. The bend die rotates and draws the tube along with it. The pressure die prevents the tube from rotating along with the bend die. The pressure die may be stationary or it may move along with tube. The pressure die provides a boost (pushes the material at the extrados of the tube) to reduce the thinning of the tube and can be very helpful when the bending angle is large and the bending radius is small [6]. A mandrel along with wiper die may be used to prevent the wrinkling and collapse of the tube. But the use of mandrel should be avoided if possible since it increases the production cost [7]. Figure 1-1 shows the tooling of rotary draw bending process. Rotary

draw tube bending provides close control of metal flow necessary for small radius and thin walled tube [5].

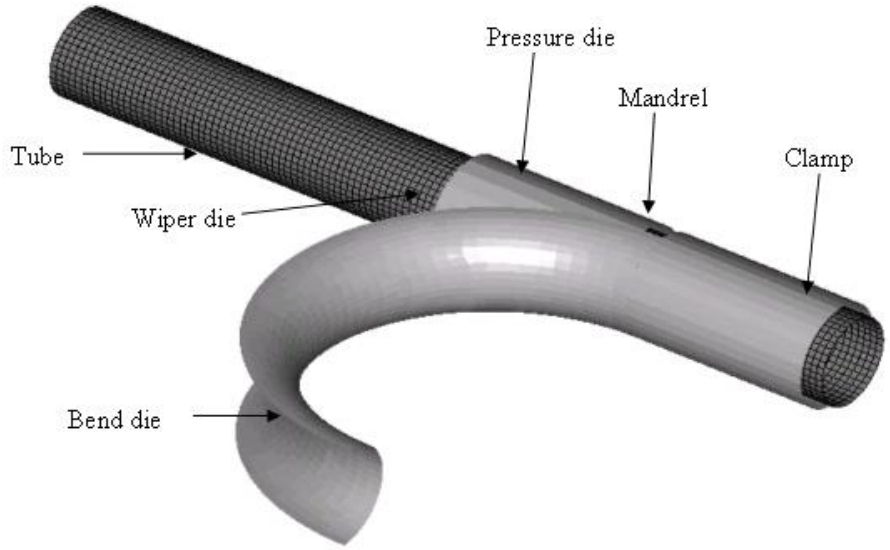

Fig. 1-1 Tooling of rotary draw tube bending process

1.1.2 Compression Tube Bending

The tooling for the compression tube bending is similar to the rotary draw tube bending. It consists of the stationary bend die, a moving wiper shoe and a clamp. The only difference between the rotary braw bending and compression bending process is that in rotary draw tube bending the bend die is movable whereas in the compression tube bending the bend die is stationary. In compression tube bending the tube is clamped

to the bending die near the rear tangent point. The wiper shoe pushes the tube along the bending die as it rotates around it. Figures 1-2a and 1-2b show the initial and final configuration of the compression tube bending.

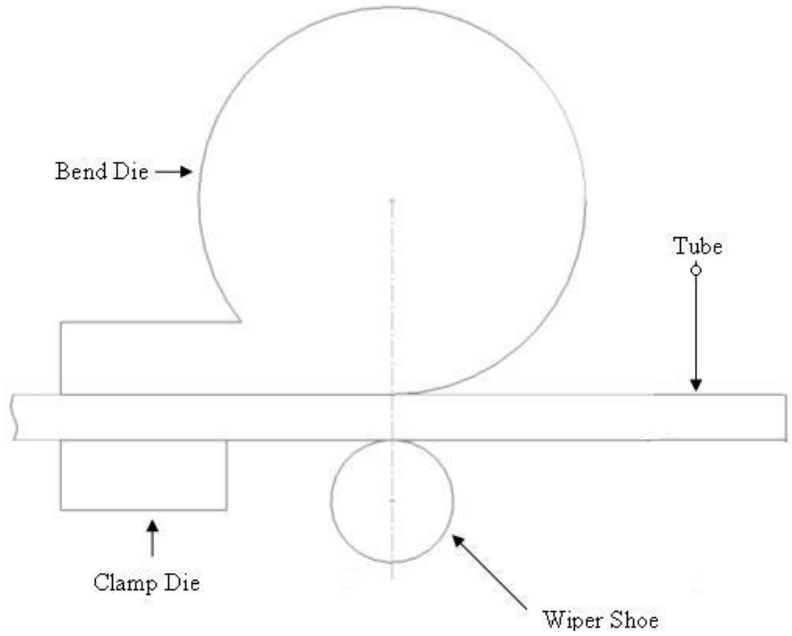

Fig. 1-2a Initial configuration of compression tube bending

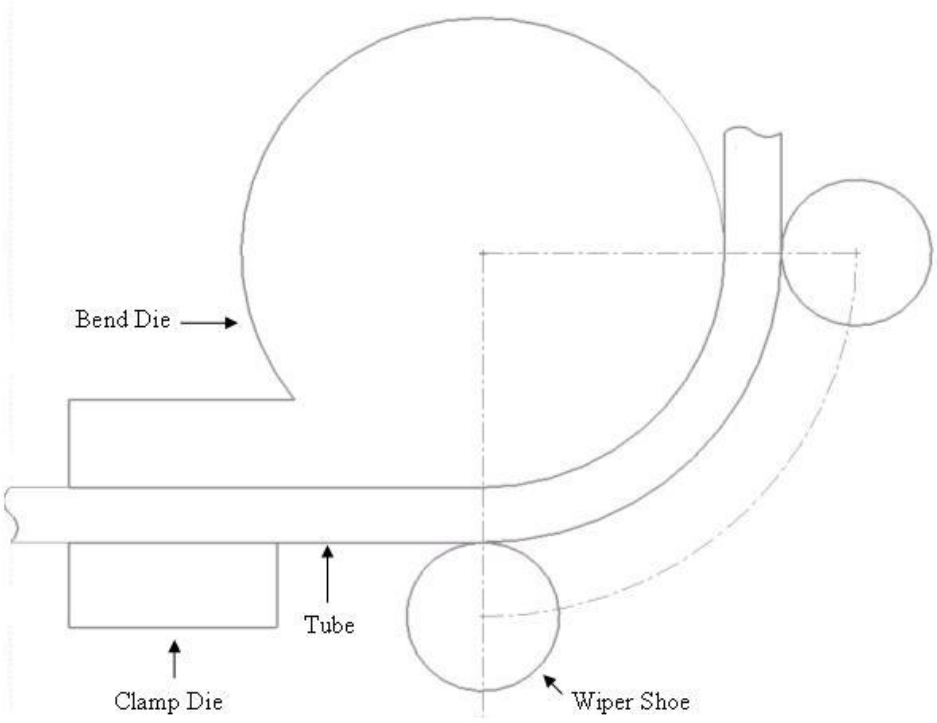

Fig. 1-2b Final configuration of compression tube bending

1.1.3 Roll Bending

The tooling for roll bending consists of three rolls of the same size arranged in a pyramid pattern, as shown in Figure 1-3. Two rolls are fixed and the third (center) roll is movable. The tube is passed through the rolls and the center roll is lowered onto the tube. This bending technique is usually employed for bending tubes of large radius, spirals and tube sections of different diameters [5].

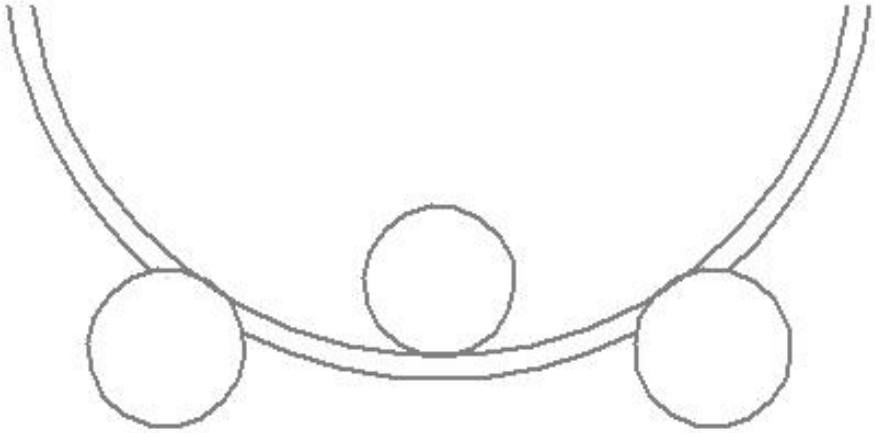

Fig. 1-3 Roll bending [5]

1.1.4 Stretch Bending

Stretch bending is one of the newer bending techniques being used in industry. In stretch bending both the inner and outer fibers of the tube are in tension. The outer fiber is stretched more than the inner fiber. In the other bending methods described above the outer fibers are in tension whereas the inner fibers are in compression. The tooling for stretch forming consists of a mandrel (bending die), jaws, and hydraulic actuators. In this process the tube is first gripped by the jaws which are mounted on hydraulic actuators. The grips also seal the ends. The tube is first stretched axially to a chosen value of tension, and then pressure is increased to the desired level while the tension is kept

constant. The mandrel then moves and bends the tube [8, 9]. Figures 1-4a and 1-4b show the initial and final configuration of stretch bending.

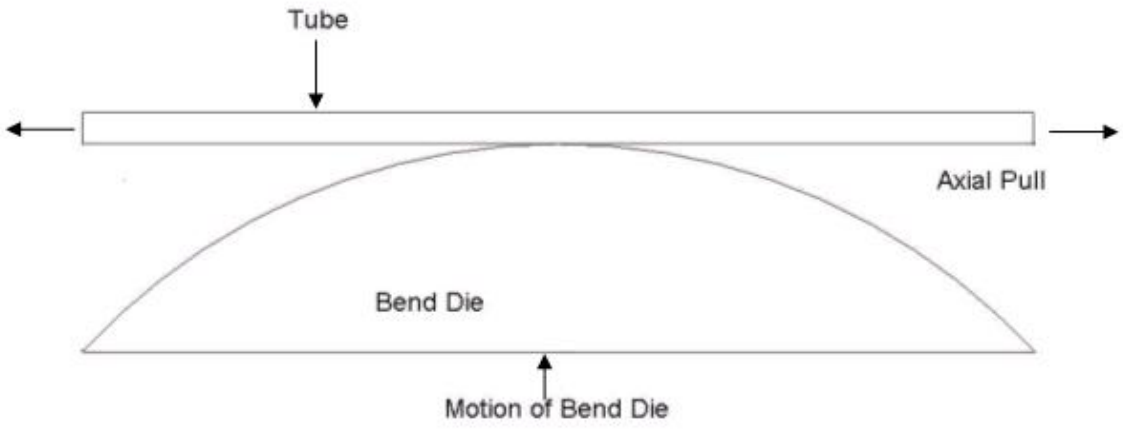

Fig. 1-4a Initial configuration of stretch bending

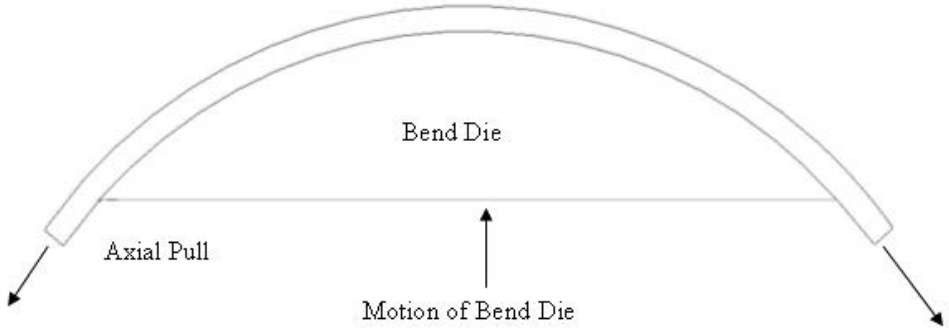

Fig. 1-4b Final configuration of stretch bending

1.2 Defects in Tube Bending

During the bending process the tube undergoes considerable in-plane distortion. The limitations in the tube bending process are distortion of cross-section, wrinkling, variation in wall thickness, springback and fracture.

1.2.1 Variation in Wall Thickness

During the bending process the bending moment induces axial forces in the inner and outer fibers. The inner and outer fibers are subjected to compressive and tensile stresses respectively. This results in thinning of the tube wall at the outer section (extrados) and thickening of the tube wall at the inner section (intrados). The wall thickness variation is shown in Figure 1-5.

1.2.2 Bursting or Fracture

The fibers at the extrados are subjected to tensile stress. When the tensile stress induced in the tube due to the bending moment at the extrados exceeds the ultimate yield strength of the material, the tube fractures at the extrados.

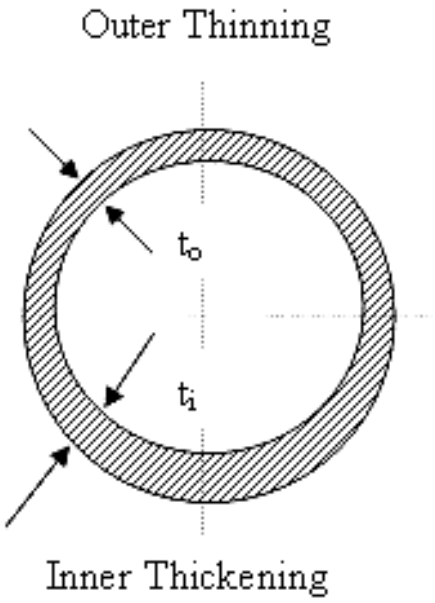

Fig. 1-5 Variation in wall thickness of the tube

1.2.3 Wrinkling

As the tube is bent, the inner surface of the tube, the intrados is subjected to compressive stress. When the tube is bent into a tight radius, it is subjected to high compressive stress in the intrados which leads to Bifurcation instability or buckling (wrinkling) of the tube. Wrinkles are wavy types of surface distortions. As tubes are used as parts in many applications where tight dimensional tolerances are desired, wrinkles are unacceptable and should be eliminated. Furthermore, wrinkles spoil the aesthetic appearance of the tube. Figure 1-6 shows tube wrinkling.

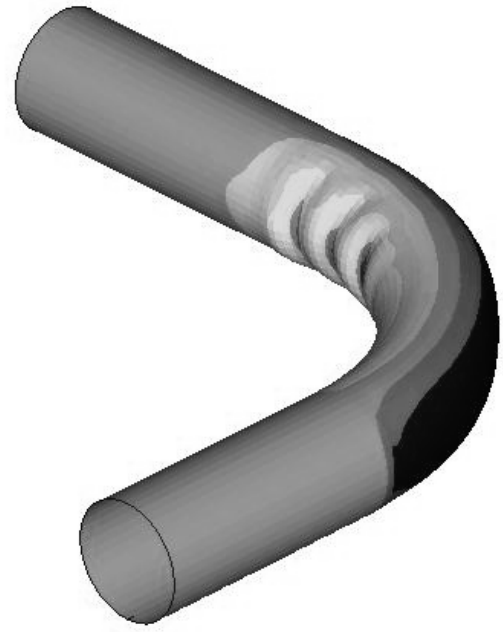

Fig. 1-6 Tube wrinkling

1.2.4 Cross Section Distortion

As described above the outer fibers of the tube are subjected to tensile stress whereas inner fibers of the tube are subjected to compressive stress. There is a tendency of fibers at both the ends to move towards the neutral axis. The outer fiber of the tube tends to move towards the neutral plane to reduce the tensile elongation. This results in the cross section of the tube being no longer circular, instead becoming oval. The common practice in industry is to provide support to the tube from inside to prevent flattening or distortion of cross section; usually a filler material or mandrel is used for that. Figure 1-7 shows the cross section distortion of tube.

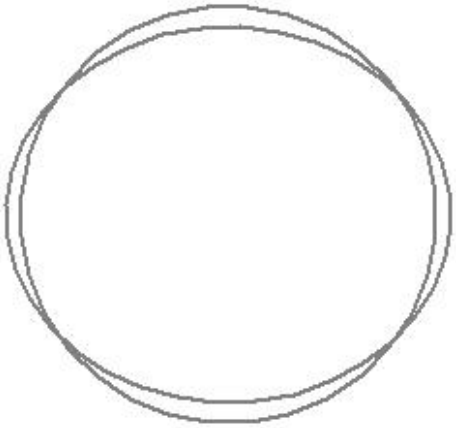

Fig. 1-7 Cross section distortion

1.2.5 Springback

After the bending process is complete and the toolings have been withdrawn the bend tube springbacks due to the elastic nature of the tube material. This is called springback or the elastic recovery of the tube. During the bending process internal stresses are developed in the tube and upon unloading the internal stresses do not vanish. After bending the extrados is subjected to residual tensile stress and the intrados is subjected to residual compressive stress. These residual stresses produce a net internal bending moment which causes springback. The tube continues to springback until the internal bending moment drops to zero. The springback angle depends on the bend angle, tube material, tube size, mandrel, machine and tooling [10]. In actual practice the amount of

springback is calculated and the tube is over bent by that amount. Figure 1-8 shows springback after the tooling has been removed.

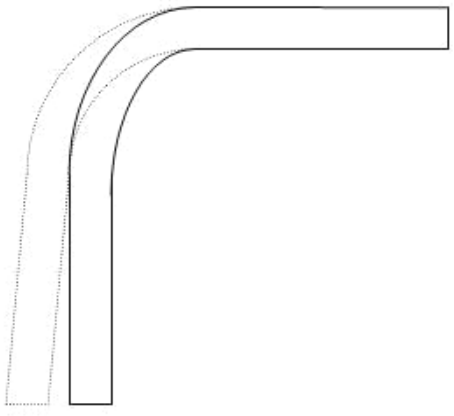

Fig. 1-8 Springback

1.3 Advantages of Additional Loading

The present study is focused on additional loading conditions in tube bending. The additional loadings considered are application of axial pull in the direction opposite to the motion of the tube, application of internal pressure and combination of internal pressure and axial pull. The application of internal pressure and axial pull either individually or in combination has various advantages when compared to the conventional bending methods.

1.3.1 Application of Axial Pull

The main goal for applying axial pull is to eliminate wrinkling, a compressive buckling problem. The application of axial pull reduces the compressive stress at the intrados and as the axial pull is increased further wrinkling can be eliminated. The advantages of using axial pull are listed below.

1. Eliminates wrinkling.
2. Reduces springback
3. Reduces tooling cost by eliminating the use of expensive mandrel and wiper die.
4. Improves bending for small bend die radius.
5. Increases versatility of the bending process.

Despite the above mentioned advantages, application of axial pull increases the cross section distortion.

1.3.2 Application of Internal Pressure

The longitudinal stress developed due to the internal pressure helps in reducing the compressive stress at intrados i.e. with proper selection of pressure wrinkling can be eliminated. The main advantages of applying internal pressure are

1. Eliminates wrinkling.
2. Reduces the cross section distortion.

3. Reduces the thinning at the extrados for small bend die radius as compared to using a mandrel.

4. Increases plastic flow due to the absence of friction between the tube and fluid.

5. Provides better contact with the tube as compared to using a mandrel.

In certain cases very high pressure may be required to eliminate wrinkling, so a combination of internal pressure and axial pull may be necessary to get the optimum results.

1.4 Research Objective

As described above, wrinkling and cross section distortion are the two most severe defects in the tube bending process. Industry practice for eliminating wrinkling is to use a mandrel along with a wiper die. Mandrel selection depends on the angle of bend, material of the tube and the degree of bend.

The present research investigates application of only axial pull, only internal pressure and combination of axial pull and internal pressure on the conventional rotary draw tube bending process. Application of axial pull in the direction opposite to the motion of the tube eliminates wrinkling. It also assists in reducing springback. Despite the fact that axial pull eliminates wrinkling and reduces springback, it further adds to the problem of cross section distortion. To eliminate the problem of cross-section distortion, a combination of axial pull and internal pressure will be employed to achieve a better

cross section of the tube. In addition to axial pull, internal pressure will be applied to the tube to eliminate wrinkling. There are four main goals in this thesis:

1. Develop an analytical model to predict the thickness distribution and cross section distortion during bending along the mid cross section of the tube for variable loading conditions. The loading conditions studied in the present research are application of axial pull in the direction opposite to the tube movement, application of internal pressure and combination of the two.

2. Develop a FEA simulation to predict the thickness distribution, effective plastic strain and cross section distortion of the along the tube during the bending process. The results obtained form the FEA simulation will be verified with published experimental results.

3. Compare the results obtained by the analytical model for different loading conditions with the results obtained from the FEA simulations.

4. Perform a parametric study using finite element simulations to investigate the effects of axial pull and internal pressure on tube bending.

The outline of the present thesis is as follows: chapter II presents the literature search on the work done on various aspects of tube bending. Chapter III presents an analytical model to predict the thickness distribution and cross section distortion of the tube during bending. Plastic deformation theory is used for the model. In chapter IV, the FEA capability is presented by comparing the results of the FEA simulation with previously published results. In chapter V, the results of the analytical model were compared for different loading conditions. First the model was compared with no additional loading

with the published experimental and numerical results. Then the results for different loading conditions predicted by the analytical model developed in chapter III are compared with the results of the FEA simulations. In chapter VI, a parametric study is conducted to study the effects of pressure and tension on the thickness, effective plastic strain and cross section distortion of the tube. Finally the conclusions are made on the basis of the present study.

CHAPTER II

LITERATURE REVIEW

In the past, researchers have worked on cross section distortion, wall thickness variation, and wrinkling issues related to pure bending of tubes. Brazier [11] studied the distortion of round tubes in elastic bending using energy minimization. Named after Brazier's work, the cross section deformation in tube bending is often called the Brazier effect. Zang and Yu [12] investigated the Brazier effect of an infinitely long, cylindrical tube under pure elastic-plastic bending. Expressions of bending moment and flattening ratio in terms of radius of curvature were obtained. Considering a finite length tube, Pan and Stelson [13] used energy method to solve for the distortion shape and wall thickness variation of plastically deformed tubes. Tang [14] developed expressions for calculating the magnitude of stresses in simple tube bending. Wall thickness change, shrinking rate at the bend section, deviation of the neutral axis, and feed preparation length were derived based on plastic deformation theories. Corona and Kyriakides [15], Kyriakides and Ju [16], and Corona and Vase [17] investigated the instability (wrinkling) of infinite length, cylindrical and square tubes under bending. Wang and Cao [18] studied wrinkling in tube bending with boundary restriction at the ends. An energy method was used to determine the critical bending radius at the onset of wrinkling as a function of tube dimensions, tooling geometry and material properties. With the advancement of computational mechanics, the finite element method has been used to simulate tube bending process. Zhan et al. [19] simulated a rotary draw tube bending process for a

thin-walled tube. It was seen that the maximal wall thinning ratio at the extrados changes only slightly, and the maximal wall thickening ratio at the intrados increases linearly with increase of bend angle. Yang et al. [7] simulated the rotary bending process and concluded that in the case of bending with mandrel, the section remained close to circular, but the thickness reduction at extrados can be significant. Tarana [6] conducted simulations of rotary draw bending and tube hydroforming processes. The influence of bending operation on hydroforming was demonstrated.

With changes in loading condition, tubes under stretch bending behave differently from those under rotary bending. Dyau and Kyriakides [20] studied the response of long, relatively thin-walled tubes bent into the plastic range in the presence of axial tension. It was found that the ovalization induced in bending with tension depends upon the loading path, the material properties, and the geometry of the tube. Miller et al. [8, 9] conducted a series of experiments on bending of rectangular tubes on a bend-stretch form-pressure machine and developed analytical models to predict the distortion, elongation, and springback of tubes as functions of the pressure, tension, and die radius. In their experiments they found that tubes can be formed without wrinkling at value of tension lower than the yield tension. Zhu and Stelson [21] studied the distortion of cross section of a rectangular tube during stretch bending. The internal pressure at which no distortion will occur was calculated from the tube thickness, die radius, and yield strength of the material.

Several important findings from the previous tube bending research motivated the present study. First, wrinkling tendency can be reduced with axial tension. While axial

tension generates larger cross section distortion, moderate internal pressure could minimize the distortion. Although better shape control is achieved, combining axial force and internal pressure could result in deteriorated wall thickness variation. Thus, the objective of the present work is to develop an analytical model to predict the shape and thickness of tubes under bending, axial force, and internal pressure. Instead of using energy minimization approach employed in most of the previous work, plastic deformation theories adapted by Tang [14] are used. Finite element simulations of rotary draw bending with and without axial force and internal pressure were conducted. The effects of additional axial force and internal pressure are presented and discussed.

CHAPTER III

ANALYTICAL MODEL

The present chapter presents an analytical model to predict wall thickness distribution along the cross section of the tube and the cross section distortion of the tube. An analytical model provides an accurate prediction of final tube geometry in a comparatively smaller computing time than that for FEA simulations. A generalized model is developed to predict the wall thickness change and cross section distortion of the tube for combined internal pressure and axial pull.

The coordinate system used in the analysis is shown in Figure 3-1. On the bending plane, a tube of radius *r* (tube center to the mid wall) and wall thickness *t* is bent over a die of radius *R* with bending angle θ. Axial force *F*, applied at the end is equal to zero in case of pure bending and bending with internal pressure only. On the cross section, the circumference of the tube is represented by span angle α. The extrados is defined by $0 \le \alpha < \pi/2$ and $3\pi/2 \le \alpha < 2\pi$. The intrados is the section where $\pi/2 \le \alpha < 3\pi/2$. Internal pressure P_i, applied to the inside surface of the tube is equal to zero in the case of pre bending and bending with axial pull only.

The pertinent assumptions for the analysis include:

1. A plane perpendicular to the tube axis before deformation remains plane and perpendicular to the axis after deformation.
2. Wall thickness of the tube is small in comparison to the length and radius of the tube. Hence deformation due to transverse shear is neglected.

3. The deformation is symmetric with respect to the x-y plane and the plane normal to x-y plane at $\theta/2$.
4. The material is incompressible, elastic strain is neglected, and work hardening is not considered.
5. Friction between the tube and tooling is neglected.
6. Neutral axis shift during pure bending (bending without additional loading) is neglected.

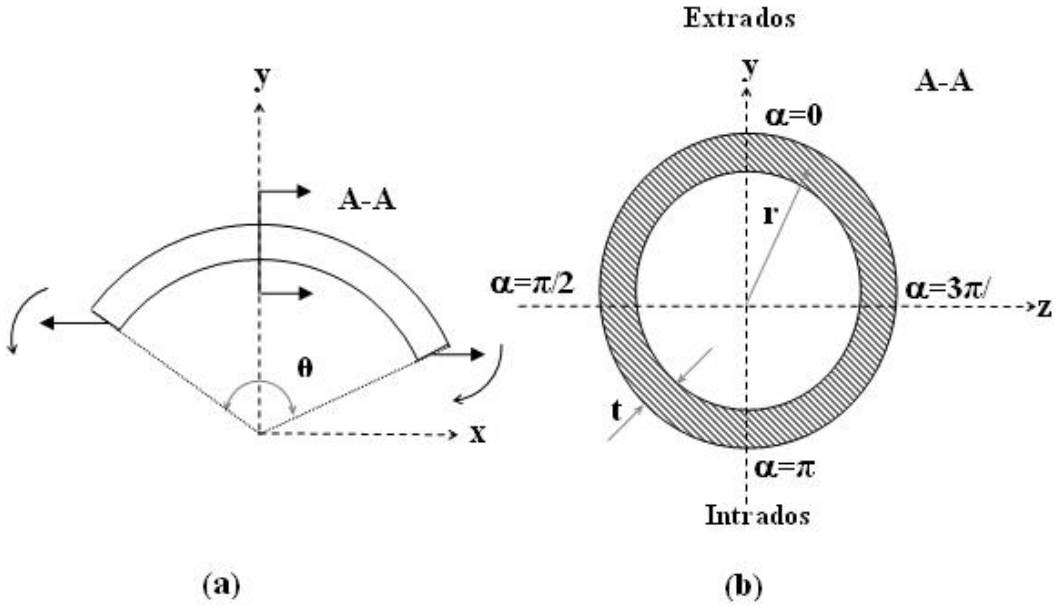

Fig. 3-1 Coordinate system of the bending analysis (a) bending plane, (b) cross section of tube

Under these assumptions, the stresses, strains, thicknesses, and distortion of the tube due to bending, axial force, and internal pressure were derived. Mathematical software Maple™ 9 is used for symbolic processing and numerical evaluation of the equations.

3.1 Axial, Circumferential, and Radial Stresses and Strains

In the case of bending with axial pull and internal pressure the tube is subjected to longitudinal stresses and circumferential stresses due to the bending moment, axial pull and the internal pressure.

3.1.1 Stresses Induced due to Bending Moment and Axial Pull

Consider a small element of the tube undergoing deformation as shown in Figure 3-2a and Figure 3-2b.

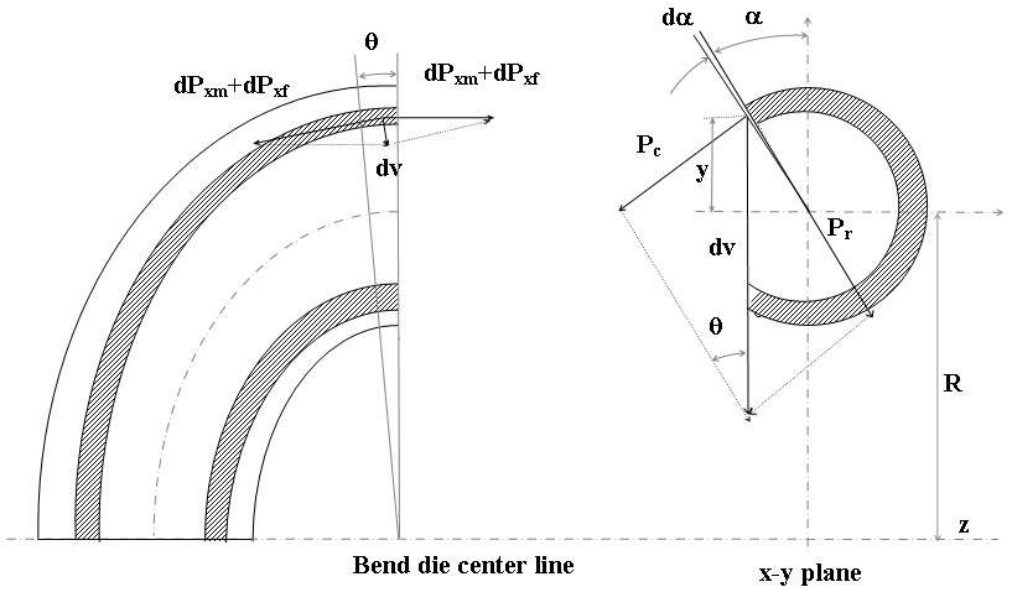

Fig. 3-2a Stress acting on a small element

The axial internal force induced in the element as a result of the bending moment is dP_{xm}:

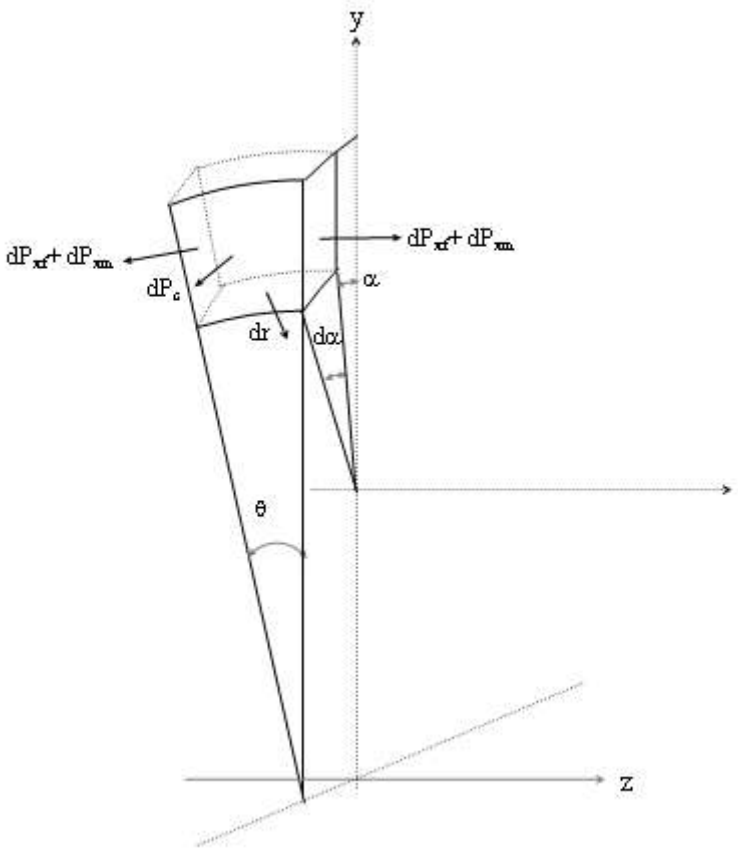

Fig. 3-2b Stress cube

$$dP_{xm} = \sigma_{xm} A = \sigma_{xm} tr(d\alpha) \tag{3-1}$$

where σ_{xm} is the axial stress induced in the tube due to bending moment and A is the cross section area. The axial force induced in the element due to the applied axial force F is dP_{xf}:

$$dP_{xf} = \frac{F}{2\pi rt} tr(d\alpha) = \sigma_{xf} tr(d\alpha) \tag{3-2}$$

where, $\sigma_{xf} = \frac{F}{2\pi rt}$ is the axial stress due to the applied axial force. Hence the resultant axial force and stress are given by

$$dP_x = dP_{xm} + dP_{xf} = (\sigma_{xm} + \sigma_{xf}) tr(d\alpha) = \sigma_x tr(d\alpha) \tag{3-3}$$

and the centripetal force dv is:

$$dv = 2dP_x \sin\frac{\theta}{2} \approx dP_x \theta \tag{3-4}$$

This centripetal force has a component in the circumferential direction:

$$dP_c = dv(\sin\alpha) = \sigma_x tr d\alpha\theta \sin\alpha \tag{3-5}$$

Following Tang's [16] approach, the circumferential force can be represented in terms of the circumferential stress σ_c:

$$dP_c = (d\sigma_c) t(R + y)\theta \tag{3-6}$$

where y is the vertical distance from the tube center to the element and $y = r\cos\alpha$ as shown in Figure 3-2. Equating (3-5) and (3-6):

$$d\sigma_c = \frac{r\sin\alpha(d\alpha)}{R + r\cos\alpha}\sigma_x \tag{3-7}$$

The circumferential stress is then obtained by integrating (3-7)

$$\sigma_c = -\sigma_x \ln\frac{R + r\cos\alpha}{R + r} \tag{3-8}$$

To simplify the expression, let

$$K = \ln\frac{R + r}{R + r\cos\alpha} \tag{3-9}$$

Therefore

$$\sigma_c = K\sigma_x \tag{3-10}$$

Without the application of axial force and internal pressure, the bending moment alone results in plastic deformation. Based on von Mises criterion:

$$(\sigma_x - \sigma_c)^2 + (\sigma_c - \sigma_r)^2 + (\sigma_r - \sigma_x)^2 = 2Y^2 \tag{3-11}$$

and $\sigma_x = \sigma_{xm}$, $\sigma_c = K\sigma_x$, $\sigma_r = 0$ yield:

$$\sigma_{xm} = \pm \frac{Y}{\sqrt{K^2 - K + 1}} \tag{3-12}$$

where Y is the yield strength of the material.
The $\pm$ sign indicates tension or compression at the extrados or intrados.

3.1.2 Stresses Induced due to Internal Pressure

Figure 3-3 shows the internal pressure P_i acting on the tube. Figure 3-4 shows the stress induced on the tube due to internal pressure. Since the wall thickness of the tube is very small in comparison to the radius of the tube, the radial stress is taken as zero i.e. $\sigma_r = 0$. σ_{xp} is the longitudinal stress induced in the tube due to the internal pressure and σ_{cp} is the hoop stress or the circumferential stress induced in the tube due to the internal pressure.

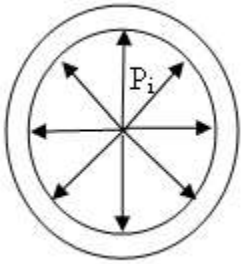

Fig. 3-3 Pressure acting on tube

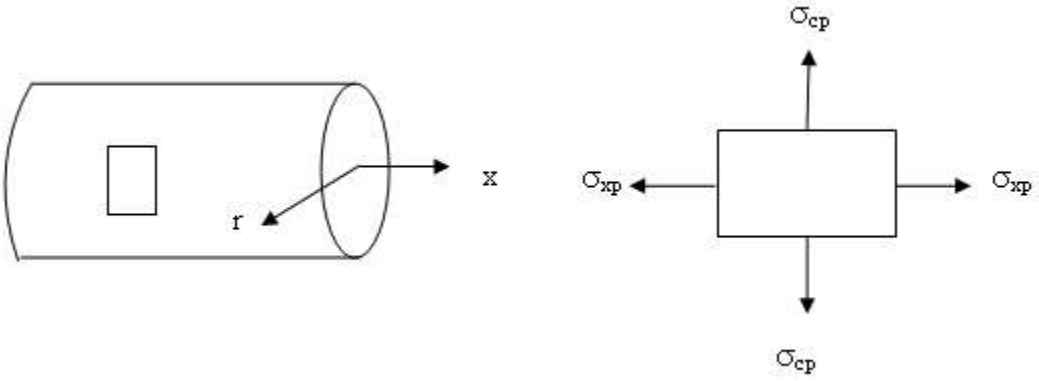

Fig. 3-4 Stress acting on the tube due to internal pressure

$$\sigma_{xp} = \frac{P_i r}{2t} \tag{3-13}$$

$$\sigma_{cp} = \frac{P_i r}{t} \tag{3-14}$$

3.1.3 Resultant Stress State

As the result, the longitudinal stress at extrados due to combined loading of bending, axial force, and internal pressure can be expressed by adding equation (3-13) to equation (3-3) and substituting equation (3-12) and $\sigma_{xf} = \frac{F}{2\pi rt}$ into equation (3-3).

$$\sigma_{xo} = \frac{Y}{\sqrt{K^2 - K + 1}} + \frac{F}{2\pi rt} + \frac{P_i r}{2t} \tag{3-15}$$

The circumferential stress is obtained by adding equation (3-14) to equation (3-10)

$$\sigma_{co} = K\sigma_x + \frac{P_i r}{t} \tag{3-16}$$

Radial stress is given by

$$\sigma_{ro} = 0 \tag{3-17}$$

As the result, the longitudinal stress at intrados due to combined loading of bending, axial force, and internal pressure can be expressed by adding equation (3-13) to equation (3-3) and substituting equation (3-12) and $\sigma_{xf} = \frac{F}{2\pi rt}$ into equation (3-3).

$$\sigma_{xi} = -\frac{Y}{\sqrt{K^2 - K + 1}} + \frac{F}{2\pi rt} + \frac{P_i r}{2t} \tag{3-18}$$

The circumferential stress is obtained by adding equation (3-14) to equation (3-10)

$$\sigma_{ci} = K\sigma_x + \frac{P_i r}{t} \tag{3-19}$$

Radial stress is given by

$$\sigma_{ri} = 0 \tag{3-20}$$

3.1.3 Neutral Axis Shift

Figure 3-5 shows the distribution of longitudinal stress across the cross section of the tube in case of pure bending. It is assumed that the tube is bent first and then axial pull is applied to the tube [24]. Due to the application of axial pull the neutral axis shifts towards the inside of the bend and with increase in the axial pull, neutral axis moves out of the plane of bending. With the application of the axial pull the neutral axis shifts by an amount e towards the center of bend. The longitudinal stress distribution for that case is shown in Figure 3-6.

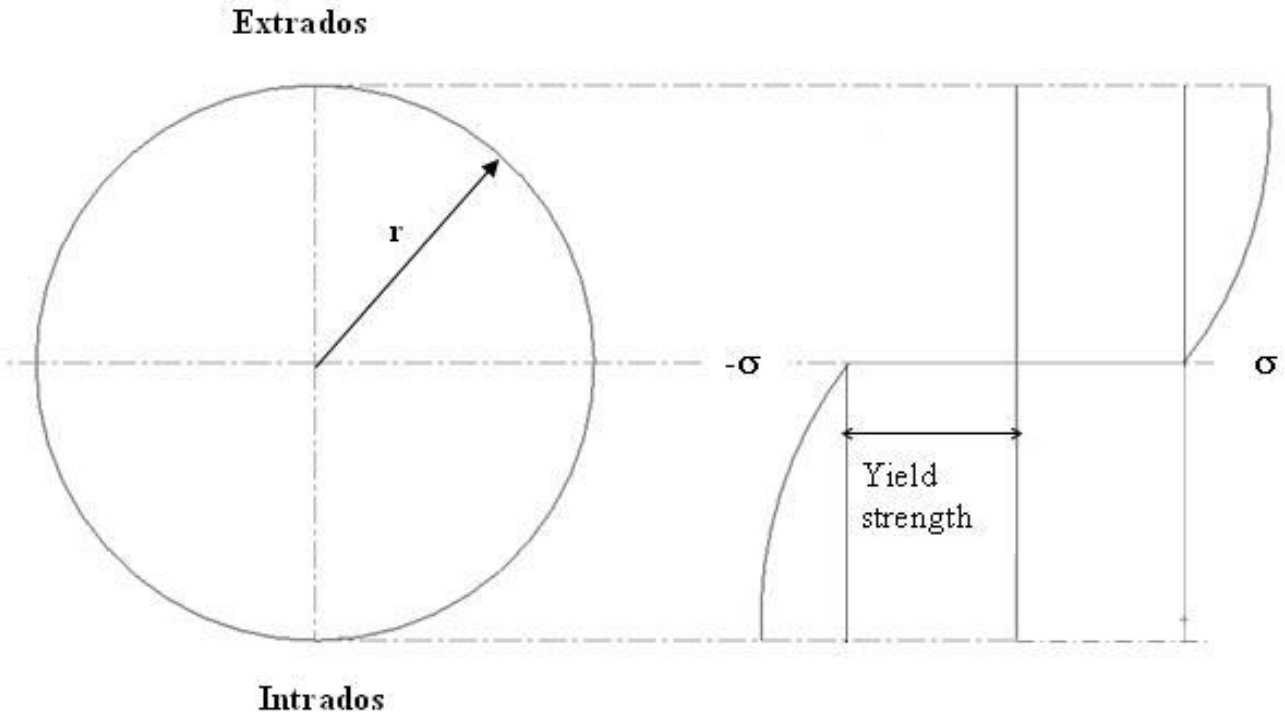

Fig. 3-5 Neutral axis for the case of pure bending

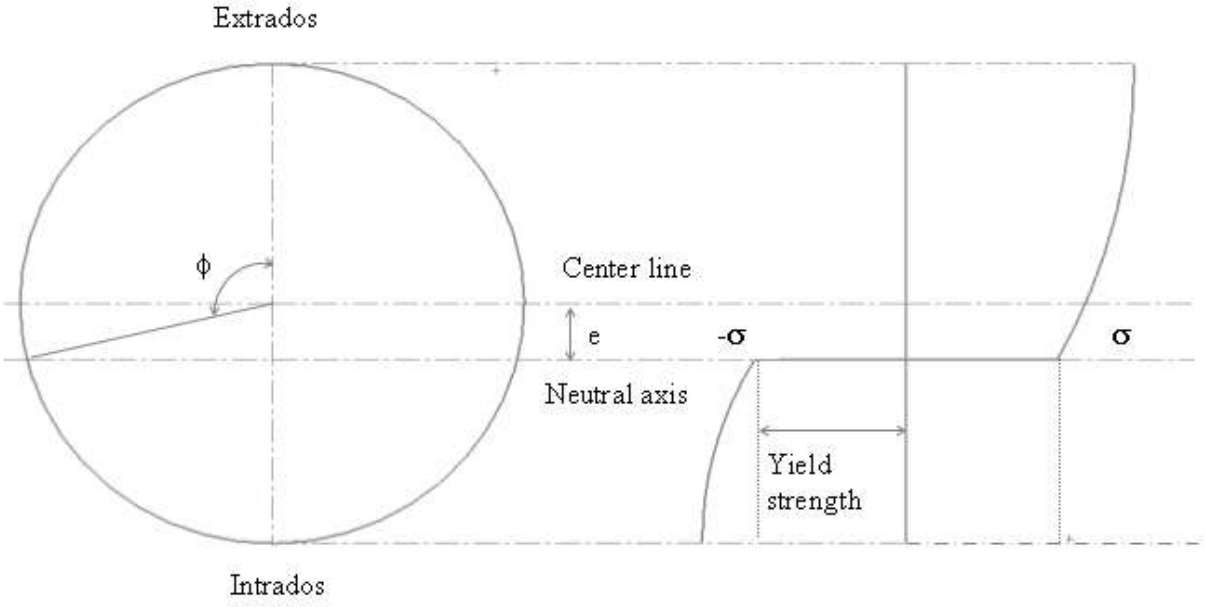

Fig. 3-6 Neutral axis shift e due to the application of axial pull

The longitudinal strain has two components- tensile strain (ε_{xt}) induced due to the axial pull, and bending strain (ε_{xb}) [12]. The tensile strain remains constant throughout the section.

$$\varepsilon_x = \varepsilon_{xt} + \varepsilon_{xb} = \frac{e}{R} + \frac{y}{R} \tag{3-21}$$

where, e is the neutral axis shift

Duncan [24] calculated the neutral axis shift in case of sheet bending on application of axial pull. The same technique is employed to calculate the neutral axis shift of the tube.

$$F = \int_0^{\phi} Yt(r\cos\alpha)d\alpha - \int_{\phi}^{\pi} Yt(r\cos\alpha)d\alpha \tag{3-22}$$

$$\phi = \sin^{-1}\left(\frac{F}{2Ytr}\right) \tag{3-23}$$

where, ϕ is the neutral axis shift in degrees.

$$y = r\cos\alpha \tag{3-24}$$

$$e = r\cos\phi \tag{3-25}$$

The resultant longitudinal strain is obtained by substituting equation (3-24) and (3-25) into equation (3-21)

$$\varepsilon_x = \frac{r}{R}(\cos\alpha + \cos\phi) \tag{3-26}$$

By flow rule, the strain state can be obtained as:

$$\varepsilon_r = \frac{2\sigma_r - (\sigma_x + \sigma_c)}{2\sigma_x - (\sigma_c + \sigma_r)}\varepsilon_x \tag{3-27}$$

$$\varepsilon_c = \frac{2\sigma_c - (\sigma_r + \sigma_x)}{2\sigma_x - (\sigma_c + \sigma_r)}\varepsilon_x \tag{3-28}$$

3.2 Wall Thickness Change and Distortion of the Cross Section

The wall thickness change and distortion of the cross section can be derived from the stresses and strains due to loading. The thickening of the intrados and thinning of the extrados are found from the radial strain:

$$t_\alpha = (1+\varepsilon_r)t \tag{3-29}$$

where t_α is the wall thickness of the tube at a given span angle α.

Radial strain at extrados is obtained by substituting equation (3-15), equation (3-16), equation (3-17) and equation (3-26) into equation (3-27)

$$\varepsilon_{\alpha\_ext} = \frac{(\sigma_{xm}+\sigma_{xf})(K+1)-\frac{P_i r}{2t}(K+3)}{(\sigma_{xm}+\sigma_{xf})(K-2)-\frac{P_i r}{2t}K}\left(\frac{r}{R}(\cos\alpha+\cos\phi)\right) \tag{3-30}$$

Substituting equations (3-30) into equation (3-29) the wall thickness distribution along the extrados is given by

$$t_{\alpha\_ext} = \left[1+\frac{(\sigma_{xm}+\sigma_{xf})(K+1)-\frac{P_i r}{2t}(K+3)}{(\sigma_{xm}+\sigma_{xf})(K-2)-\frac{P_i r}{2t}K}\left(\frac{r}{R}(\cos\alpha+\cos\phi)\right)\right]t \tag{3-31}$$

Radial strain at intrados is obtained by substituting equation (3-18), equation (3-19), equation (3-20) and equation (3-26) into equation. (3-27)

$$\varepsilon_{\alpha\_\mathrm{int}} = \frac{(\sigma_{xm}-\sigma_{xf})(K+1)-\frac{P_i r}{2t}(K+3)}{(\sigma_{xm}-\sigma_{xf})(K-2)-\frac{P_i r}{2t}K}\left(\frac{r}{R}(\cos\alpha+\cos\phi)\right) \tag{3-32}$$

Substituting equation (3-32) into equation (3-29) the wall thickness distribution along the extrados is given by

$$t_{\alpha\_\mathrm{int}} = \left[1+\frac{(\sigma_{xm}-\sigma_{xf})(K+1)-\frac{P_i r}{2t}(K+3)}{(\sigma_{xm}-\sigma_{xf})(K-2)-\frac{P_i r}{2t}K}\left(\frac{r}{R}(\cos\alpha+\cos\phi)\right)\right]t \tag{3-33}$$

The cross section distortion is caused by the circumferential stress on the tube. Substituting equations (3-15), (3-16), (3-17), (3-26) into (3-28), the circumferential strain along the extrados can be calculated by:

$$\varepsilon_{c\_ext} = -\frac{\left(\sigma_{xm}+\sigma_{xf}\right)\left(2K-1\right)+\frac{P_i r}{t}\left(K+\frac{1}{2}\right)}{\left(\sigma_{xm}+\sigma_{xf}\right)\left(K-2\right)+\frac{P_i r}{2t}K}\left(\frac{r}{R}\left(\cos\alpha+\cos\phi\right)\right) \tag{3-34}$$

Substituting Equations (3-18), (3-19), (3-20), (3-26) into (3-28) the circumferential strain along the intrados can be calculated by:

$$\varepsilon_{c\_\mathrm{int}} = -\frac{\left(\sigma_{xm}-\sigma_{xf}\right)\left(2K-1\right)-\frac{P_i r}{2t}\left(K+\frac{1}{2}\right)}{\left(\sigma_{xm}-\sigma_{xf}\right)\left(K-2\right)-\frac{P_i r}{2t}K}\left(\frac{r}{R}\left(\cos\alpha+\cos\phi\right)\right) \tag{3-35}$$

It is reasonable to estimate the cross section distortion from the tube radii calculated from the circumferential strain around the tube ($0 \le \alpha < 2\pi$):

$$r_\alpha = \left(1+\varepsilon_c\right)r \tag{3-36}$$

Substituting equation (3-34) in (3-36) the radius of tube at the outside of the bend is calculated by

$$r_{\alpha\_ext} = \left[1-\frac{\left(\sigma_{xm}+\sigma_{xf}\right)\left(2K-1\right)+\frac{P_i r}{t}\left(K+\frac{1}{2}\right)}{\left(\sigma_{xm}+\sigma_{xf}\right)\left(K-2\right)+\frac{P_i r}{2t}K}\left(\frac{r}{R}\left(\cos\alpha+\cos\phi\right)\right)\right]r \tag{3-37}$$

Substituting equation (3-35) in (3-36) the radius of tube at the inside of the bend is calculated by

$$r_{\alpha\_\text{int}} = \left[1 - \frac{\left(\sigma_{xm} - \sigma_{xf}\right)\left(2K-1\right) - \frac{P_i r}{2t}\left(K + \frac{1}{2}\right)}{\left(\sigma_{xm} - \sigma_{xf}\right)\left(K-2\right) - \frac{P_i r}{2t}K} \left(\frac{r}{R}\left(\cos\alpha + \cos\phi\right)\right) \right] r \qquad (3\text{-}38)$$

CHAPTER IV

FINITE ELEMENT ANALYSIS

Finite element simulations were used to obtain the thickness distribution of the tube, maximum effective plastic strain induced in the tube and the distortion of the cross section of the tube during the bending process. Simulations were carried on using Finite Element Analysis (FEA) solver LS-DYNA [24]. HyperMesh [25] and HyperView were used for pre and post processing of the model. Appendix A, p. 74 describes step by step procedure to construct the input deck for the rotary draw tube bending simulation using HyperMesh. The input deck is presented in Appendix B, p. 83. The FEA simulation technique was validated by comparing the results with that of a previously published work on rotary draw tube bending. This is important to show simulation capability and get accurate results. Two simulations were carried out for the validation purpose. The tooling for the first simulation was carried out using bend die, clamp die and pressure die bending with simulation was carried out based on the geometric and material property used by Khodayari [26] in his experiment. The results of the second simulation were compared with the simulation results of Shr [27]. The rigid toolings for the second simulation consisted of bend die, clamp die, pressure die, mandrel and wiper die. In this the pressure die exerted a pressure of 50 MPa on the tube. Since in the present study internal pressure is applied to the tube, the technique of applying pressure was validated in the second simulation.

4.1 Validation without Mandrel

The tooling consisted of bend die, clamp die, and pressure die. The material and geometric properties are listed in table 4-1.

Table 4-1 Material and geometric properties used by Khoyadari [26]

Parameter	Magnitude
Outside diameter of the tube (mm)	20
Thickness of the tube (mm)	1.5
Radius of bend die (mm)	50
Yield strength of tube material (MPa)	270
Young's Modulus of tube material (MPa)	219,400
Tangent modulus of tub material (MPa)	900
Poisson's ratio	0.3
Coefficient of friction between tube and bend die	0.1

The thickness distribution and cross section distortion are shown in Figure 4-1 and 4-2 respectively. It is seen that the thickness reduction at extrados predicted by Khoyadari was 9 % while the FEA simulation predicted 9.07 %. At intrados Khoyadari predicted an increase of 11 % while the FEA results predicted 12.8 %. The maximum cross section distortion predicted by Khoyadari was 10 % while the FEA simulation predicted 6.2%. Simulation with different value of coefficient of friction was done and it was found that for coefficient of friction of 0.3 the cross section distortion was 8.7 %.

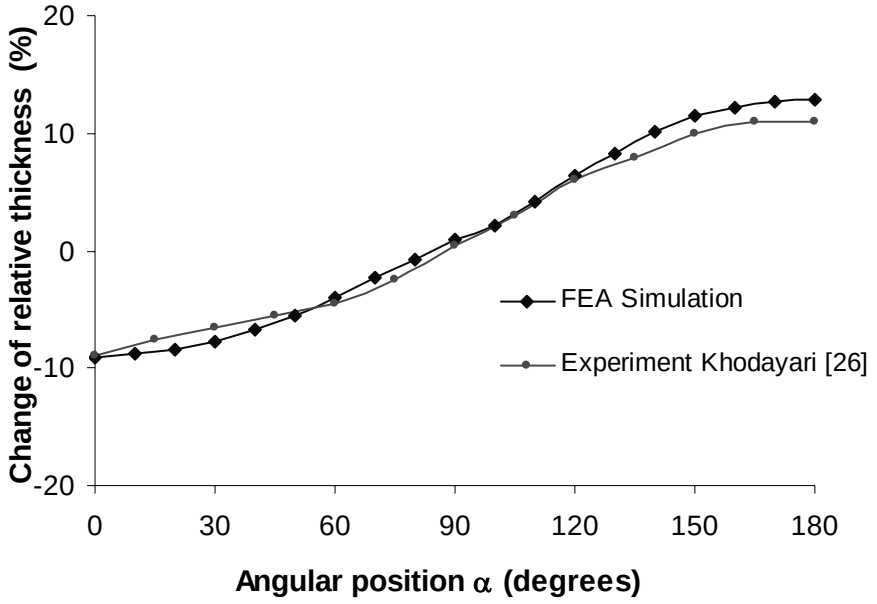

Fig. 4-1 Comparison of change in relative thickness obtained from FEA simulations with experimental values of Khodayari [26]

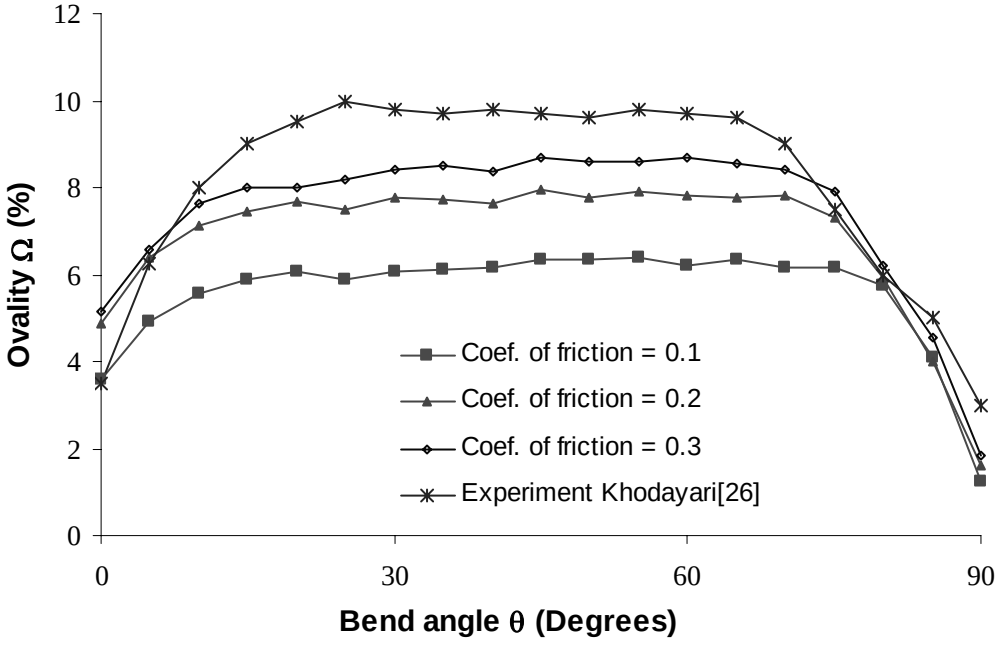

Fig. 4-2 Comparison of ovality obtained from FEA simulations with experimental values of Khodayari[26]

4.2 Validation with Mandrel

Stainless Steel SS304 was the material used for the tube. Table 4-2 shows the mechanical property of Stainless Steel SS304 used for the simulation. Table 4-3 lists the Simulation parameters used in the analysis. Geometry of the tube is shown in table 4-4.

Table 4-2 Material property of Stainless Steel SS304 (Roll formed and laser welded)

Material Property	Value
Young's Modulus E (GPa)	210
Poisson's Ratio ν	0.3
Strain Hardening coefficient K (MPa)	1451
Strain hardening exponent n	0.6
Initial strain ε_0	0.06

Table 4-3 Simulation parameters

	Value
Bend Die Radius/ Centerline Radius R (mm)	171.45 (3D)
Pressure Die Pressure (Mpa)	50.00
Mandrel type used in simulation	Plug Mandrel with wiper die
Position of mandrel relative to tangent point (mm)	4.43
Mandrel- tube inside surface clearance (mm)	0.286

Table 4-4 Geometry of tube

	Value
Initial Tube length L_0 (mm)	498.000
Initial tube outside diameter OD (mm)	57.150
Mean Radius of the tube r (mm)	27.146
Initial wall thickness of the tube t (mm)	2.858

The deformation of the tube at different bending angles is shown in Figure 4-3.

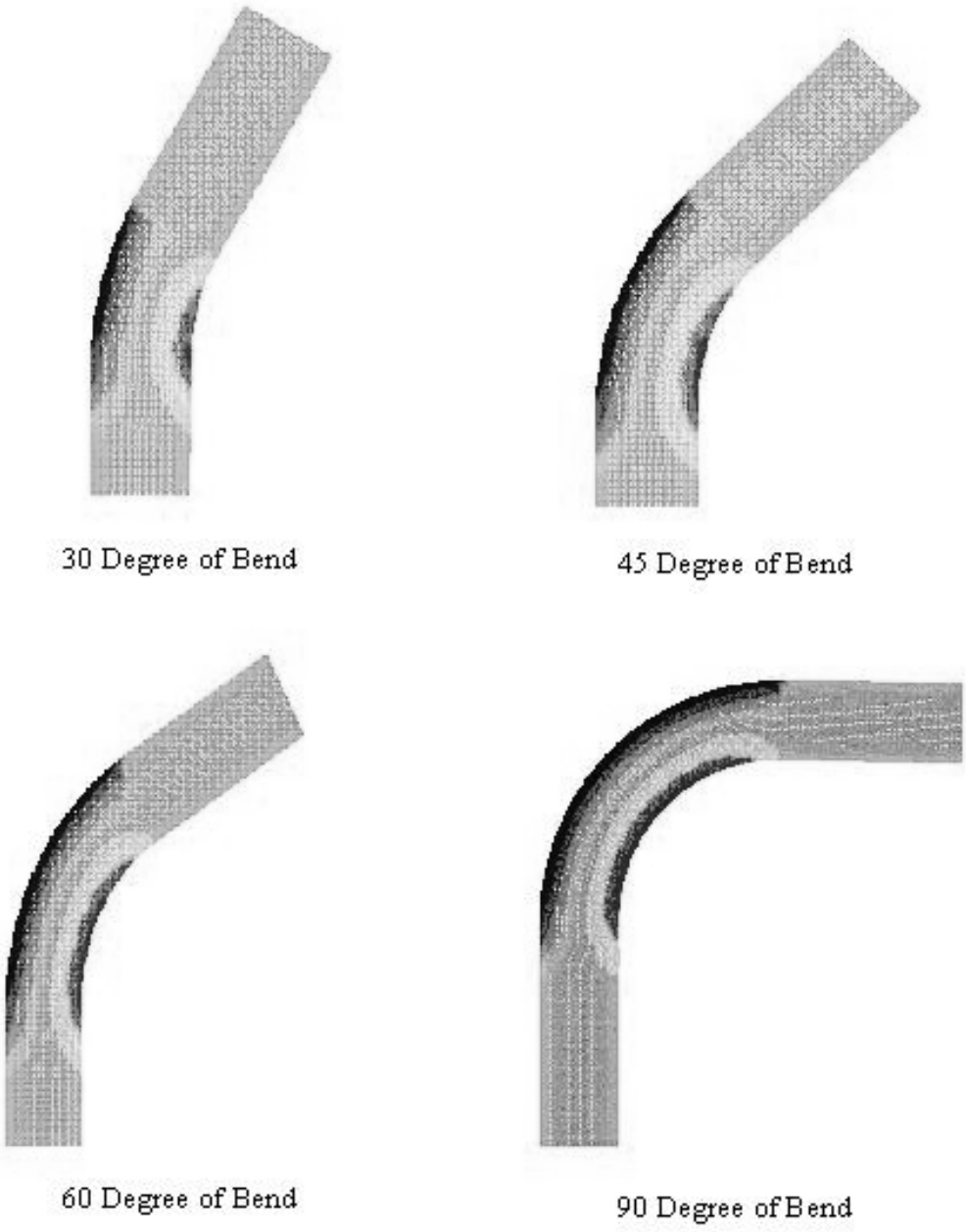

Fig. 4-3 Deformation of tube as it is bent in to different bending angles

4.2.1 Effective Plastic Strain

Effective plastic strain distribution at the extrados for 90^o bend is shown in Figure 4-4. It is seen that the stress at the clamped region remains zero in the FEA simulation where as it has a very small magnitude in Shr's simulation. The difference is due to the contact card used for clamping the tube to the bend die. In the present simulation the nodes of the tube near the clamp die are constrained to the clamp. The maximum effective plastic stress predicted by Shr is 0.1688 at extrados whereas for the FEM simulation it is 0.1666.

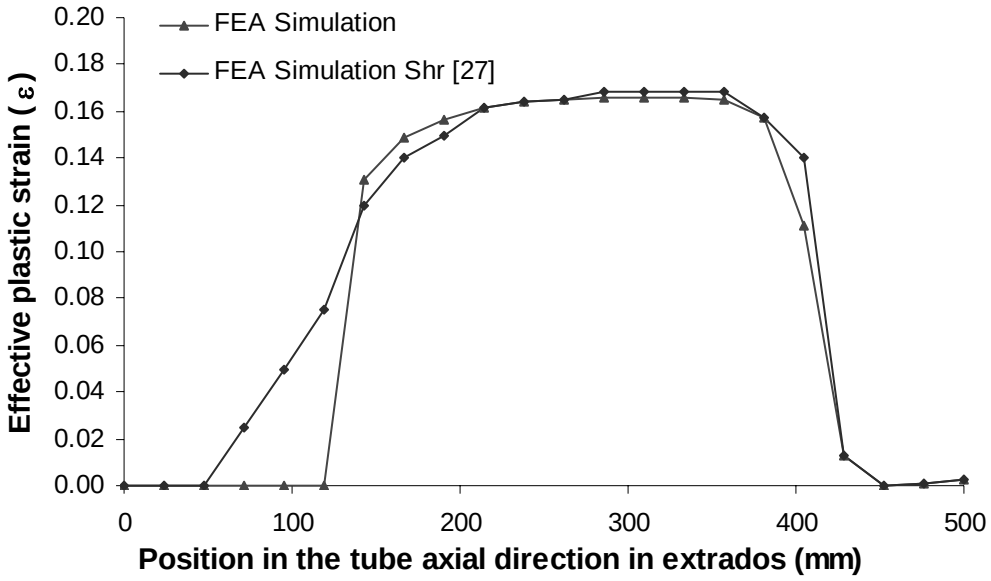

Fig. 4-4 Effective plastic strain distribution at the extrados along the length of the tube

Effective plastic strain distribution at the intrados is shown in Figure 4-5. Again it is seen that the stress at the clamped region remains zero in the FEM simulation where as it has a very small magnitude in Shr's simulation. The difference is due to the contact card used for clamping the tube to the bend die. The maximum plastic effective strain predicted by Shr is 0.1581 at intrados whereas for the FEM simulation it is 0.1645.

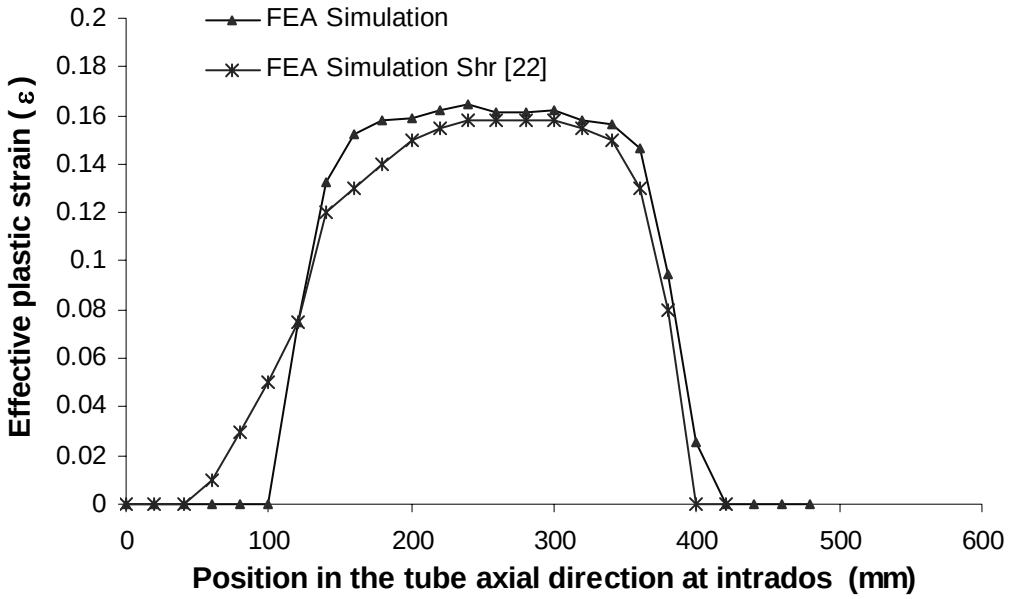

Fig. 4-5 Effective plastic strain distribution at the intrados along the length of the tube

4.2.2 Change in Relative Thickness

Change in relative thickness of the tube on the mid cross-section for a 90^o bend is shown in Figure 4-6. At intrados, an increase in thickness predicted by Shr was 8.64%

where as the FEA simulation predicted it as 9.25%. The maximum thickness reduction at extrados was 6.89% whereas Shr predicted it to be 7.28%.

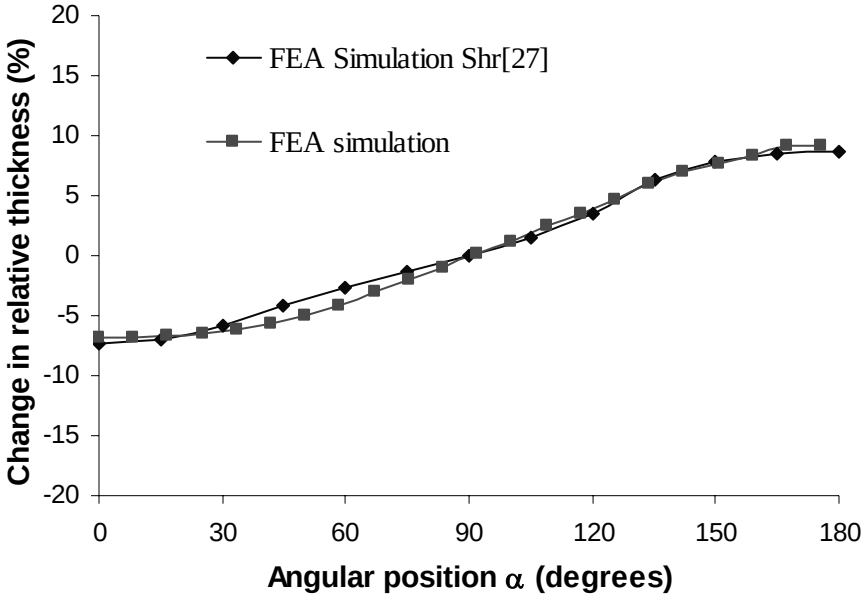

Fig. 4-6 Thickness distribution of the tube on the mid cross-section of 90^{o} bend

CHAPTER V

MODEL PREDICTIONS

The present chapter compares the wall thickness and cross section distortion for the different loading conditions predicted from the analytical model and the FEA analysis. In the first section of the chapter the wall thickness and cross section distortion predicted by the analytical model are compared for the case of pure bending with the numerical and experimental results of Pan et al. [13]. The wall thickness distribution and cross section distortion predicted by the analytical model and FEA simulation are compared with the experimental results of the Khodayari [26] for the case of pure bending. In the second section the wall thickness distribution and cross section distortion prediction form the analytical model is compared with the results of the FEA simulation for different loading conditions. In the third section wall thickness distribution and cross section distortion results obtained from the FEA simulations are compared for bending with mandrel, internal pressure and combination of axial pull and internal pressure.

5.1 Comparison of Analytical, Numerical and Experimental Results

The model prediction is compared to the analytical and experimental results from Pan and Stelson [13]. The tube parameters are listed in Table 5-1. As shown in Figure 5-1, Pan and Stelson's model over predicted the thinning and under predicted the thickening. The

wall thickness prediction from the present model is in good agreement with the experimental results. Table 5-2 compares the wall thickness predicted by the analytical model and Pan's results.

Table 5-1 Geometric and material properties used by Pan et al. [13]

Parameter	Magnitude
Diameter of the tube (mm)	25.4
Wall thickness of the tube (mm)	2.92
Radius of bend die (mm)	50.8
Yield strength of tube material (MPa)	270

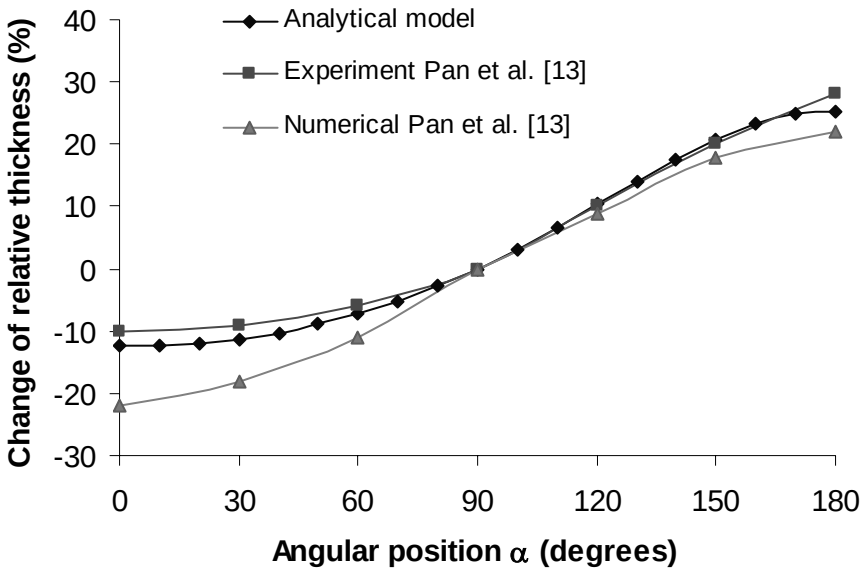

Fig. 5-1 Comparison of the wall thickness prediction by analytical model with experimental results and numerical model of Pan et al. [13]

Table 5-2 Comparison of change in relative wall thickness predicted by Pan et al. [13] and analytical model

Angular Position	Change of Relative Wall thickness (%)		
	Analytical Model	Pan et al. [13]	
		Experiment	Numerical
0	-12.49%	-10 %	-22 %
180	25.38%	28 %	22 %

For cross section distortion, the severity of distortion is defined by ovality:

$$\Omega = \frac{D_{\max} - D_{\min}}{D_0} \times 100\% \qquad (5\text{-}1)$$

where $D_{\max}$ and $D_{\min}$ are the major and minor axes of the deformed tube respectively; D_0 is the original tube diameter. The experiments showed that $5\% \le \Omega_{\exp} \le 20\%$. Pan and Stelson's model predicted the distortion at different cross sections with the ovality of $0\% \le \Omega \le 15\%$. The present model predicts only the cross section with the most significant distortion at $\Omega = 9\%$. The friction between the workpiece and tooling could contribute to this discrepancy.

The tube and tooling parameters for the tube bending experiments conducted by Khodayari [26] are listed in table 4-1. Finite element simulation was also conducted. As shown in Figure 5-2, the model predictions agree well with the finite element simulation and experimental results. Thinning at the extrados, $t_0 < t$, and thickening at the intrados, $t_\pi > t$, can be observed. Also note that $t_{\pi/2} = t_{3\pi/2} = t$ as the model assumes symmetric

deformation with respect to x-y plane and no neutral line shift in pure bending. Flattening of the extrados can be expected since, from Equation (3-36), $r_0 < r$ and $r_{\pi/2} = r_{3\pi/2} > r$.

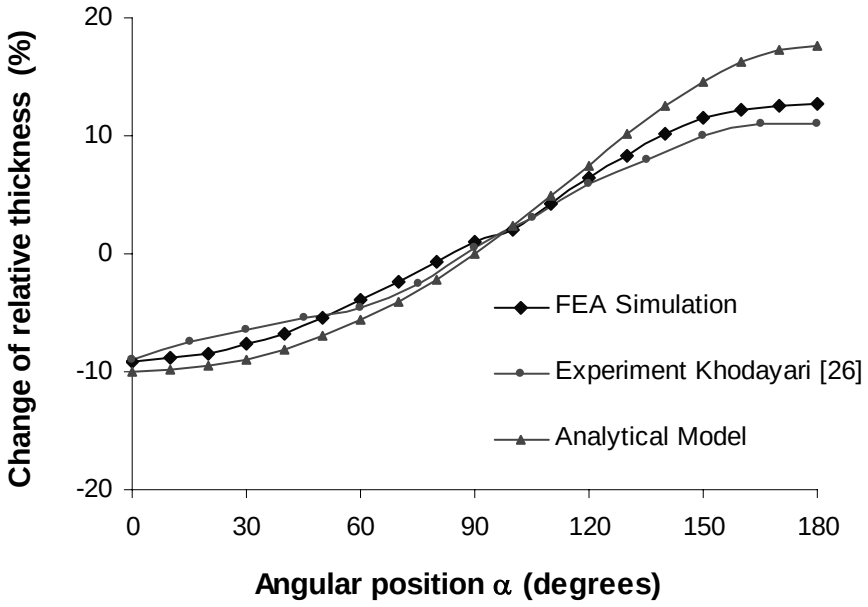

Fig. 5-2 Comparison of the wall thickness prediction by analytical model with experimental results of Khodayari [26] and FEA Simulation

The ovality is calculated at $\Omega = 6\%$ for analytical model compared to that of the experiment $\Omega_{\exp} = 10\%$. The difference may due to the friction condition between tube and tooling. Simulating tube bending with different coefficient of friction values, Fig. 5-3 shows that, at different cross sections, the ovality increases with coefficient of friction. The cross section distortion for coefficient of friction of 0.1 was 6.43% and for coefficient of friction 0.3 was 8.70%. The present model assumes no frictional effect and thus under-

estimates the severity of cross section distortion. Another possible source of error is the simplification of the distortion function, Equation (4-36).

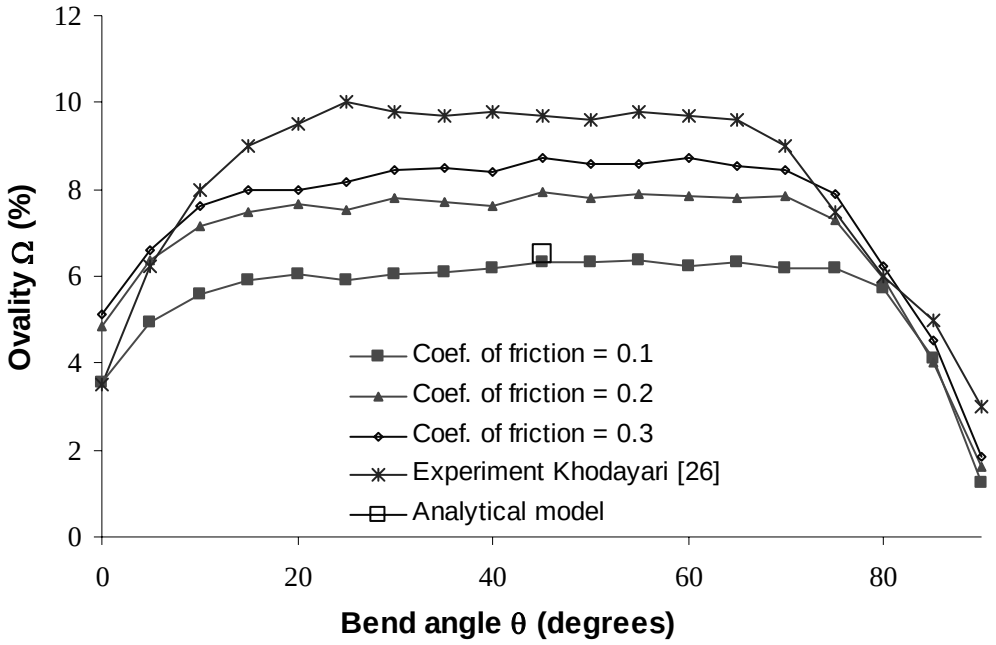

Fig. 5-3 Comparison of cross section distortion of tube obtained from FEA simulation for different values of coefficient of friction with experimental value Khodayari [26] and analytical model

5.1 Application of Additional Loading

Finite element analysis was conducted for the different loading conditions i.e. with application of axial pull, internal pressure and combination of axial pull and internal pressure. The wall thickness and cross section distortion were tabulated at the mid cross

section i.e. at 45^o for the 90^o bend. The results obtained form the analytical model is compared with the FEA results.

5.2.1 Application of Axial Pull

The effects of stretching and internal pressure on tube bending are demonstrated in the following example. For general bending, the minimum bending radius – the radius which does not yield wrinkling, can be estimated using a simple tooling design guideline [11]:

$$\frac{R}{OD} \geq 2 \qquad (5\text{-}2)$$

Based on this guideline, a small die radius which could result in wrinkling was used to bend a tube with the geometry and material properties listed in Table 5-3.

Table 5-3 Geometric and material properties of the tube

Parameter	Magnitude
Diameter of the tube (mm)	57.15
Mean radius of tube (mm)	27.15
Wall thickness of the tube (mm)	2.858
Radius of bend die (mm)	142.87
Pressure die Pressure (MPa)	50
Yield strength of tube material (MPa)	210
Young's Modulus of tube material (GPa)	210

Simulating the bending process using LS-DYNA, wrinkling is observed as shown in Figure 5-4.

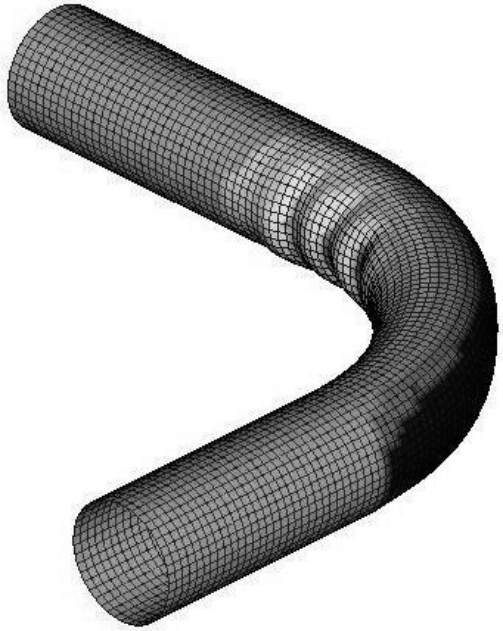

Fig. 5-4 FEA simulations for 90 degree bend showing wrinkling in the tube. The tube and geometric and material property used in simulation are listed in table 5-3

Another simulation showed that applying an axial force of 12.9 kN at the tube end near the pressure die will eliminate the wrinkling (Figure 5-5). The wall thickness and cross section distortion predicted by FEA and the analytical model are shown in Figures 5-6 and 5-7. At intrados the increase in wall thickness predicted from analytical model was 10.94% and 9.38% from FEA simulation. Wall thickness reduction prediction at extrados was 12.57% from analytical model and 8.99 % from FEA simulation. While no wrinkling, the cross section distortion is significant with ovality $\Omega = 11.3\%$ from FEA simulation and 7.3% form the analytical model. Figure 5-8 shows the change in radius of the tube along the span angle.

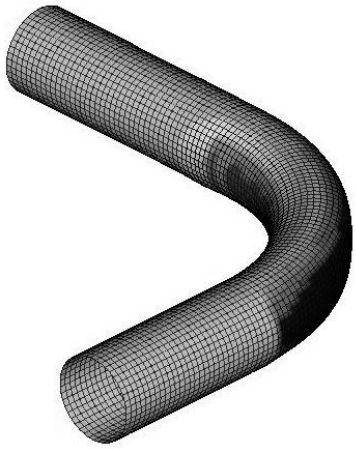

Fig. 5-5 Application of axial pull eliminates wrinkling

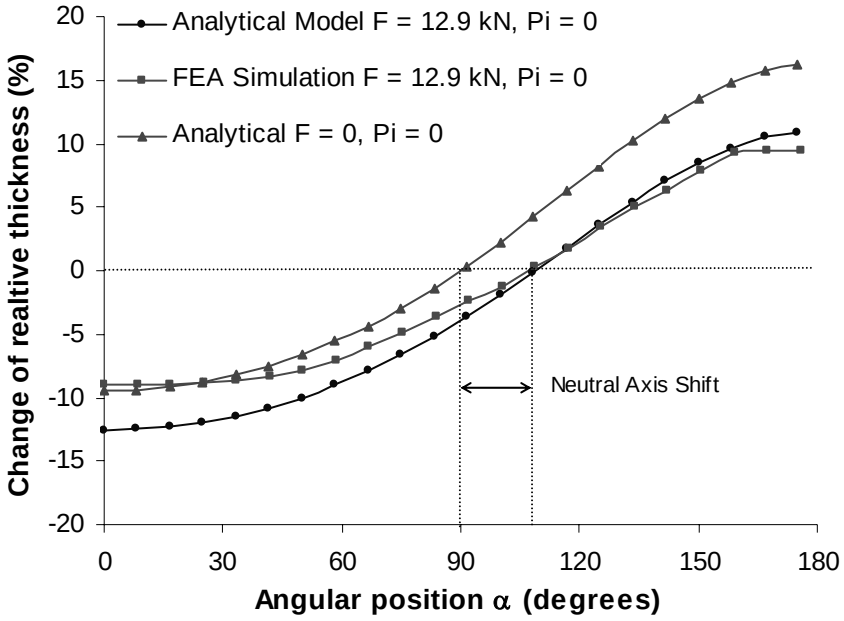

Fig. 5-6 Comparison of the wall thickness prediction by analytical model (axial pull 12.9 kN and no internal pressure) with FEA Simulation (axial pull 12.9 kN and no internal pressure) and analytical model (no axial pull and no internal pressure)

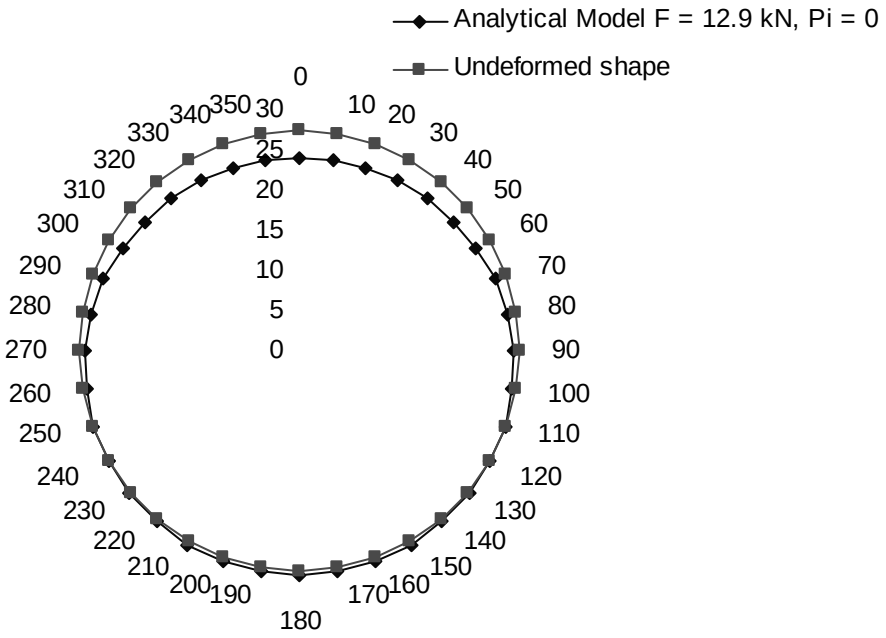

Fig. 5-7 Polar plot of the cross section prediction by analytical model (axial pull 12.9 kN and no internal pressure) with undeformed tube

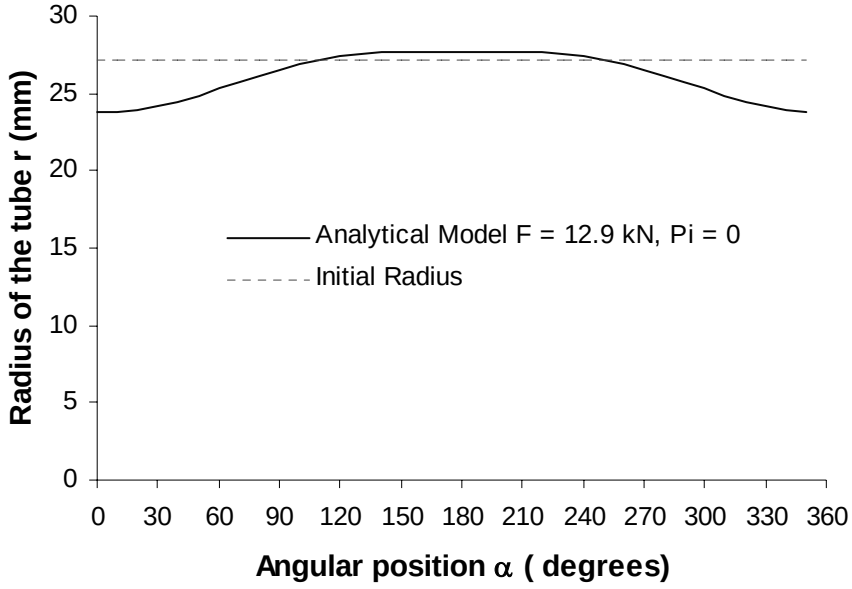

Fig. 5-8 X-Y Plot of the radius prediction by analytical model for axial pull of 12.9 kN and no internal pressure with initial radius of tube

5.2.2 Application of Internal Pressure

To prevent the tube from wrinkling and to reduce cross section distortion, internal pressure can be used. It was found that with 10 MPa internal pressure, wrinkling is eliminated. The analytical and FEA predictions of the wall thickness and cross section distortion are shown in Figures 5-9 and 5-10. At intrados the increase in wall thickness predicted from analytical model was 9.43% and 8.01% from FEA Simulation. The wall thickness reduction prediction at extrados was 14.77% from analytical model and 9.24% from FEA simulation.

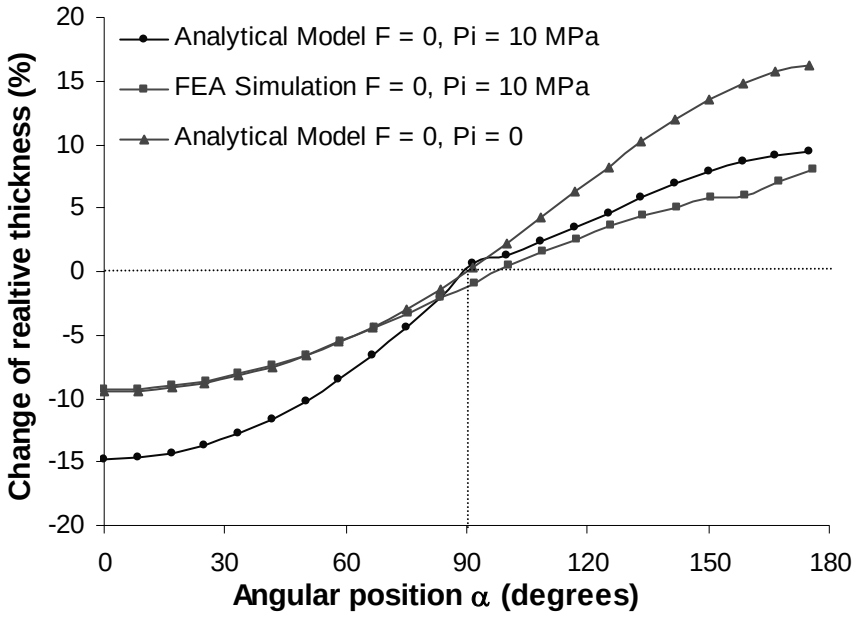

Fig. 5-9 Comparison of the wall thickness prediction by analytical model (no axial pull and internal pressure of 10 MPa) with FEA Simulation (no axial pull and internal pressure of 10 MPa) and analytical model (no axial pull and no internal pressure)

The cross section distortion prediction was 3.22% from analytical model and 4.21% from FEA simulation. From the results it is seen that internal pressure provides better cross section than the cross section obtained from bending of tube in presence of axial pull.

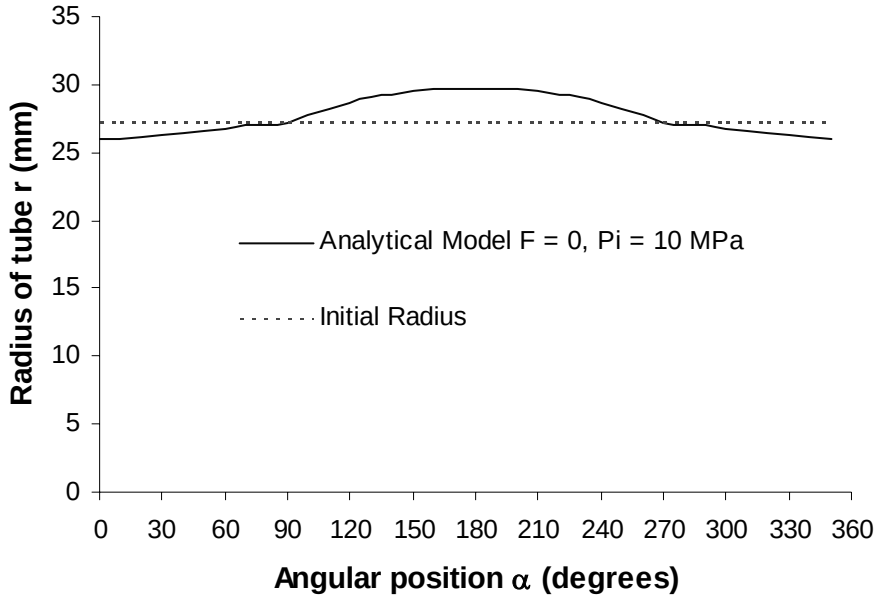

Fig. 5-10 Comparison of the radius prediction by analytical model (no axial pull and internal pressure of 10 MPa) with undeformed tube

5.2.3 Application of Internal Pressure and Axial Pull

Figures 5-11 and 5-12 show the effects of applying tension and internal pressure simultaneously during bending. At intrados the increase in wall thickness predicted from analytical model was 8.88% and 8.71% from FEA Simulation. The wall thickness reduction prediction at extrados was 15.11% from analytical model and 11.09% from FEA simulation. The cross section distortion prediction was 3.69% from analytical and 2.8% from FEA simulation. Clearly it can be seen that with application of both internal pressure and axial pull wrinkling can be eliminated and a near circular cross section can be achieved but the thinning will be more when compared to bending with only internal pressure.

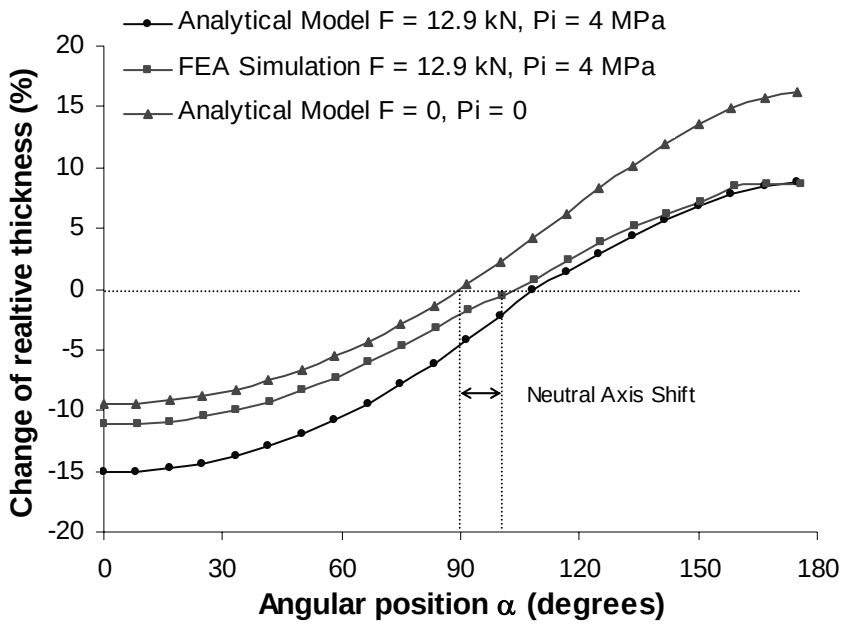

Fig. 5-11 Comparison of the wall thickness prediction by analytical model (axial pull 12.9 kN and internal pressure of 4 MPa) with FEA Simulation (axial pull 12.9 kN and internal pressure of 4 MPa) and analytical model (no axial pull and no internal pressure)

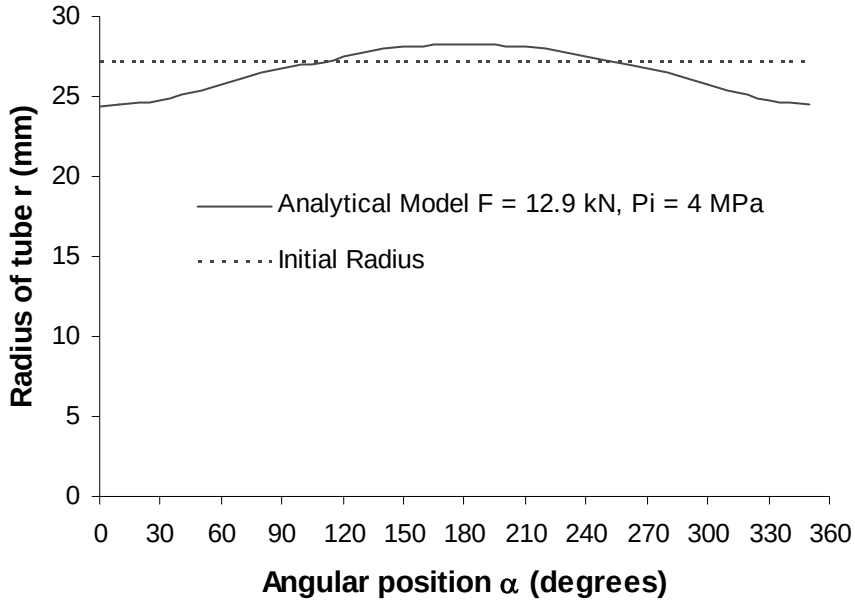

Fig. 5-12 Comparison of the radius prediction by analytical model (axial pull of 12.9 kN and internal pressure of 4 MPa) with undeformed tube

Results from both FEA simulations and analytical model show that bending with only internal pressure and bending with combined tension and internal pressure reduce cross section distortion and reduce wall thickness at intrados. The use of fluid mandrel is limited by the capacity of pressure intensifier. For the case of close bend radius high pressure may be required to eliminate wrinkling. In such case comparatively small value of internal pressure in combination with axial pull may be used to eliminate wrinkling.

In all cases, it is found that the analytical model predictions are close to the FEA predictions. It is seen that at the extrados the analytical model over predicts thinning. This is because the analytical model does not take into account the boost of 50 MPa provided by the pressure die. A FEA simulation with axial pull of 12.9 kN was conducted with no

pressure die boost. Figure 5-13 shows the wall thickness prediction of the tube. The maximum reduction of wall thickness at extrados predicted by FEA simulation with pressure die boost was 8.99% and without boost was 10.11%. The analytical model prediction was 12.57%.

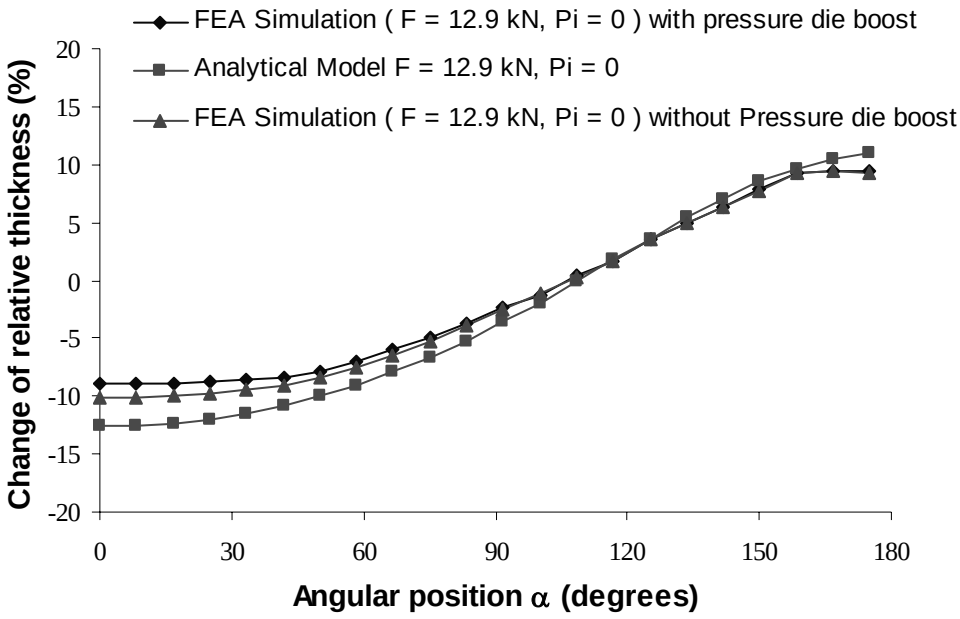

Fig. 5-13 Comparisons of wall thickness prediction by analytical model (axial pull of 12.9 kN and no internal pressure) with FEA simulation with and without Pressure die boost of 50 MPa

5.3 Comparison of Wall Thickness Distribution for Different Bending Methods

The figure 5-14 compares the wall thickness distribution for bending with a plug mandrel, internal pressure and combination of internal pressure and axial pull. It is seen from the results that at extrados the increase in wall thickness in case of internal pressure

and combination of axial pull and internal pressure was limited to 8.5% and 9% but in the case of the bending with mandrel it was 11%. At extrados the reduction in wall thickness in the case of bending with internal pressure was limited to 9.2% but it was nearly 11% in the other two cases.

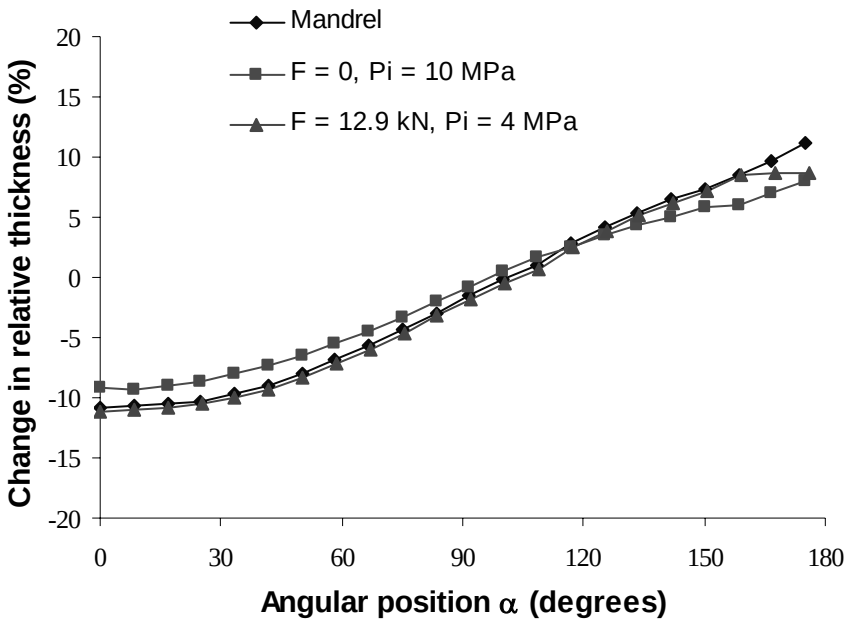

Fig. 5-14 Comparison of wall thickness distribution for bending with mandrel, internal pressure and combination of internal pressure and axial pull

CHAPTER VI

PARAMETRIC STUDY OF PROCESS PARAMETERS

A parametric study was conducted to study the effect of process parameters such as internal pressure and axial pull on the final wall thickness and cross section distortion of the tube. For the study two types of simulation were carried out. In the first type the axial pull was kept constant and the internal pressure was varied. In the second type the internal pressure was kept constant and the axial pull was varied.

6.1 Effect of Axial Pull

Simulations were carried out for six different values of pressure 0, 1, 2, 3, 4 and 5 MPa and four different values of axial pull: 12.90 kN, 15.05 kN, 17.20 kN, 19.35 N. It was seen that the wall thickness at the intrados and extrados decreases with increase in the axial pull. This is shown in figures 6-1 and 6-2.

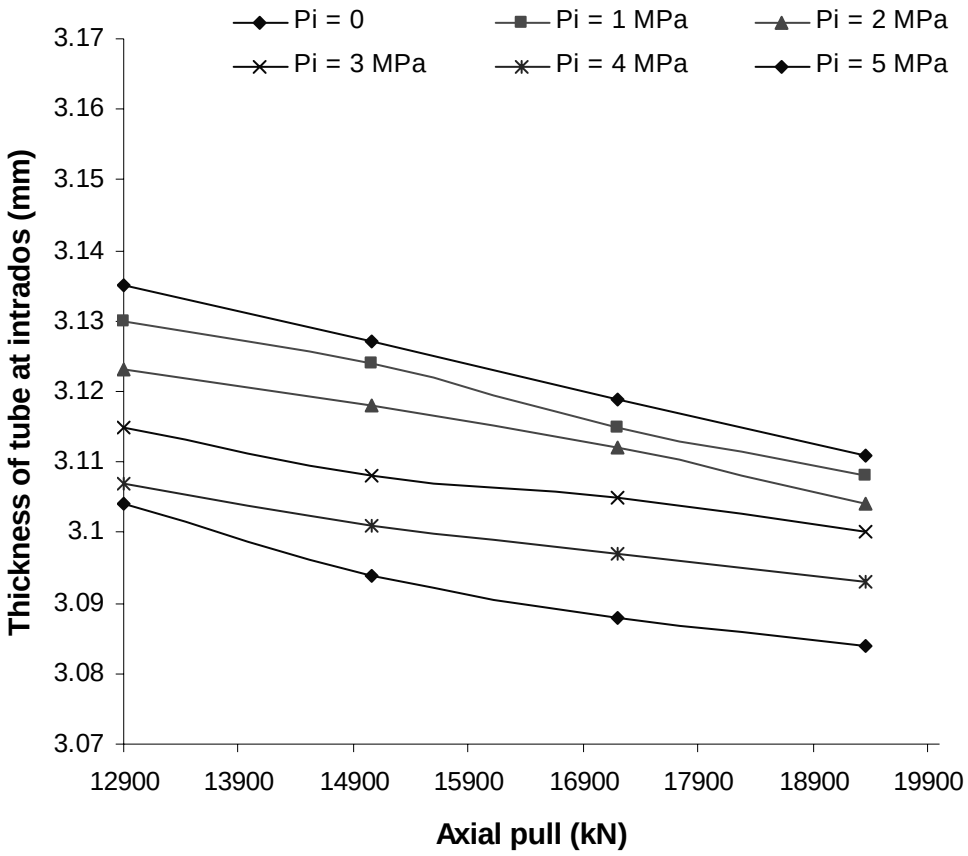

Fig. 6-1 Comparison of maximum wall thickness at intrados at constant pressure for increasing value of axial pull

From the two curves it is seen both at extrados and at intrados the wall thickness reduced with increase in the axial pull. The change in wall thickness at both extrados and intrados both follow a linear pattern. The slope of the wall thickness change at the intrados is sharp when compared to the slope of wall thickness change at the intrados. This implies with the increase in axial pull the rate of reduction in wall thickness is greater at intrados than extrados.

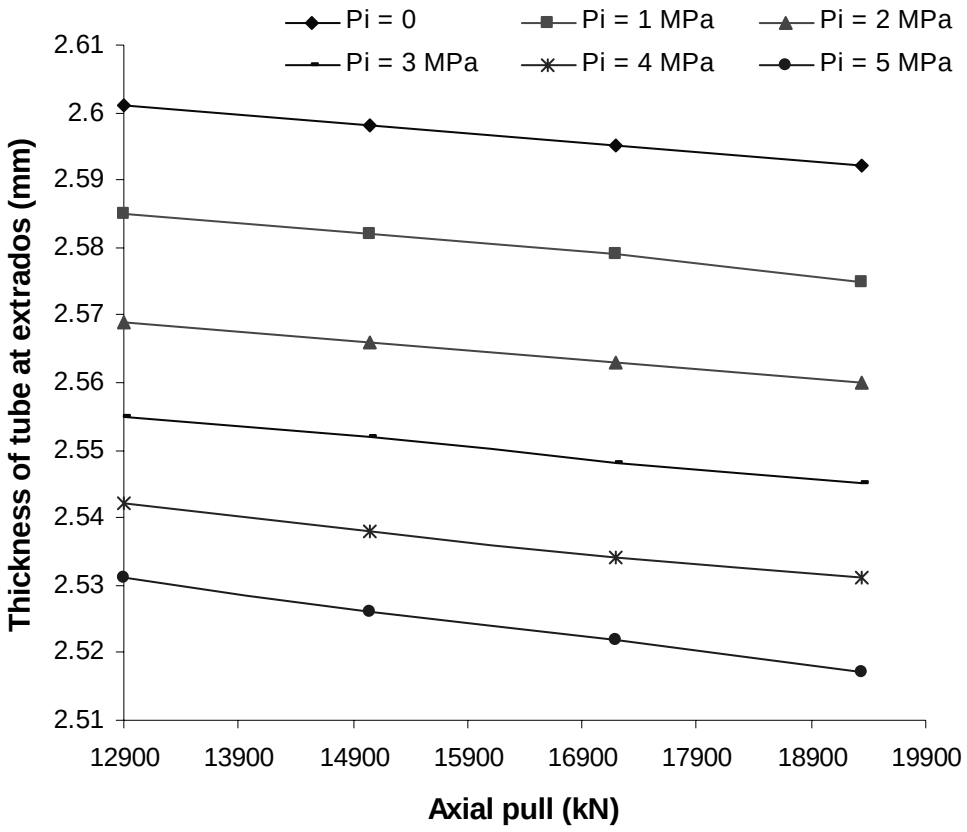

Fig. 6-2 Comparison of minimum wall thickness at extrados at constant pressure

The cross section distortion with variation in axial pull is shown in figure 6-3. It was seen that cross section distortion increased with increase in the axial pull.

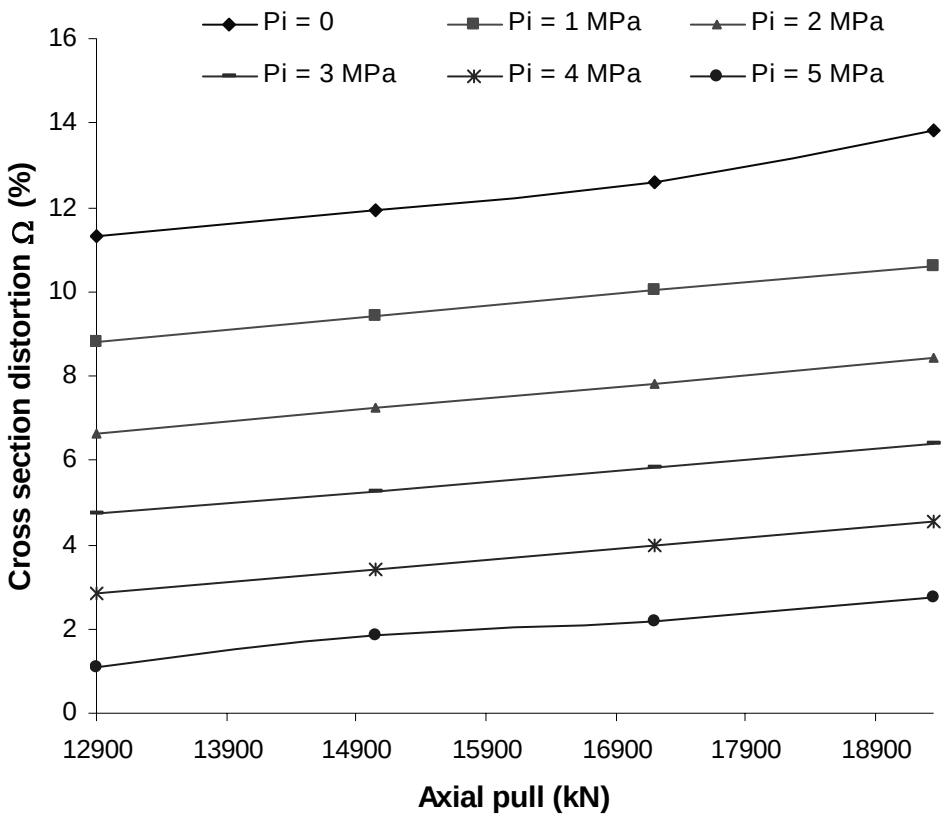

Fig. 6-3 Comparison of cross section distortion at constant pressure

6.2 Effect of Internal Pressure

It was seen that the wall thickness at the intrados decreases with increase in the internal pressure. Figure 6-4 shows the variation in maximum wall thickness with increasing pressure. The minimum wall thickness with variation in internal pressure is shown in figure 6-5. The minimum wall thickness at extrados decreases with increase in internal pressure.

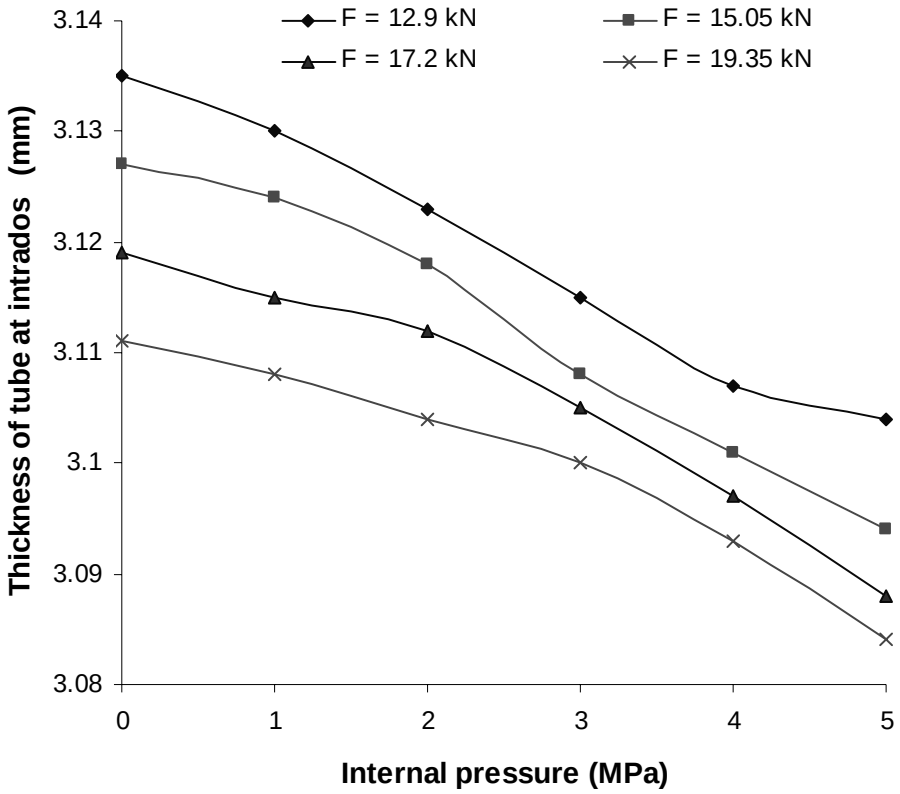

Fig. 6-4 Comparison of maximum wall thickness at intrados at constant axial pull for increasing value of internal pressure

From the two curves it is seen both at extrados and at intrados the wall thickness reduced with increase in the axial pull. The change in wall thickness at both extrados and intrados both follow a linear pattern. The slope of the wall thickness change at the extrados is sharp when compared to the slope of wall thickness change at the intrados. This indicates with the increase in internal pressure the rate of reduction in wall thickness is greater at extrados than intrados.

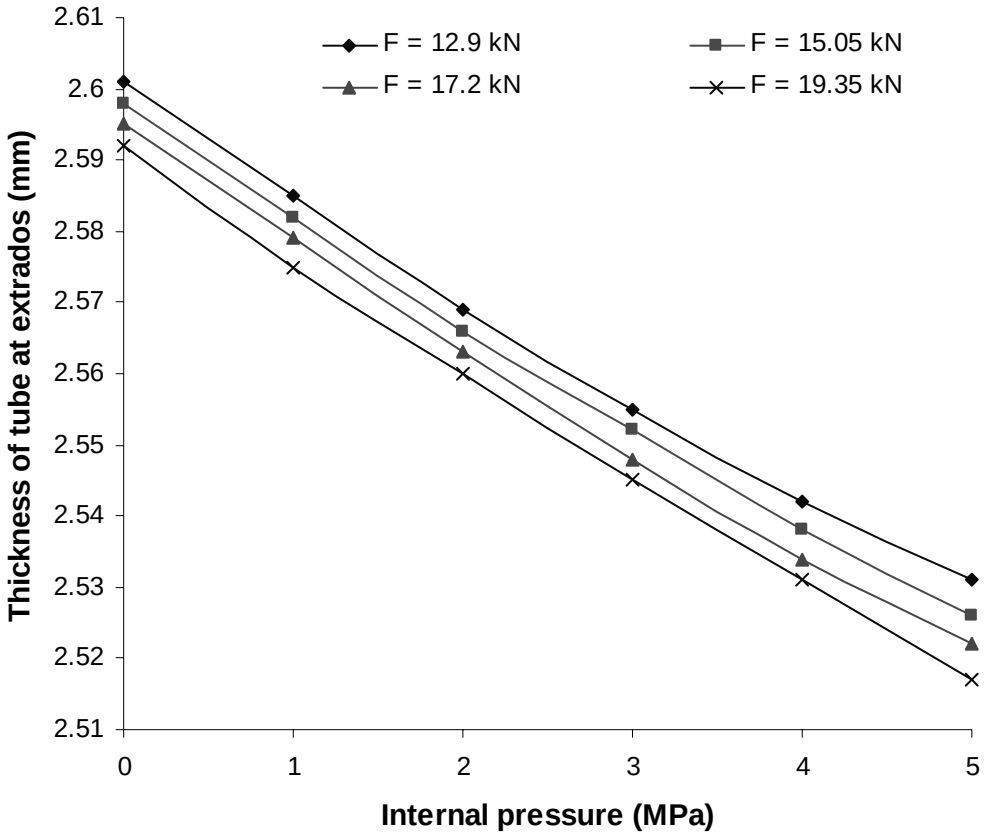

Fig. 6-5 Comparison of maximum wall thickness at extrados at constant axial pull for increasing value of internal pressure

The cross section distortion of tube with variation in internal pressure is shown in figure 6-6. It was seen that the cross section distortion decreased with increase in the internal pressure. But with further increase in internal pressure the cross section distortion increased.

From the parametric study it can be concluded that with an optimum value of pressure and axial pull wrinkling can be eliminated and the cross section of the tube can be maintained circular.

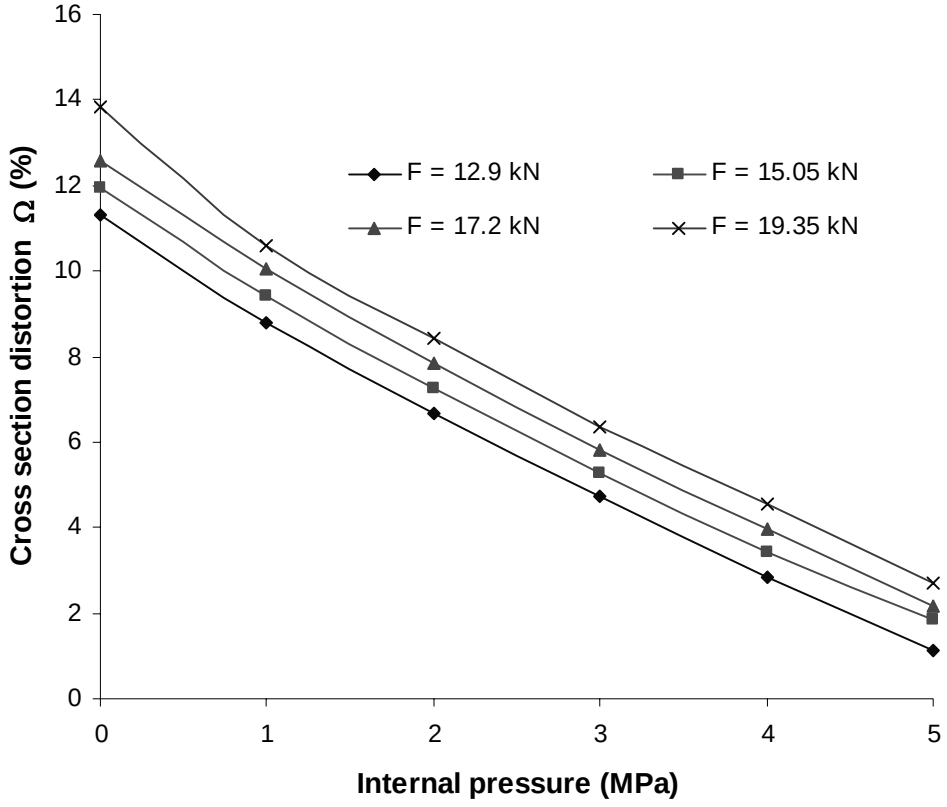

Fig. 6-6 Comparison of cross section distortion at constant axial pull for increasing value of internal pressure

CHAPTER VII

CONCLUSIONS

Stretch bending tends to minimize wrinkling and can reduce springback. By applying fluid pressure during bending, the wrinkling tendency and cross section distortion of the tube are reduced. Thus, this approach can be used for bending a thin walled tube over a small die radius, which cannot be achieved with a traditional tube bending process.

In this paper, the problem of tube bending with internal pressure and axial stretching has been investigated analytically and numerically. The objective of the study is to develop a tool to accurately predict the wall thickness variation and cross section distortion of the tube under different loading conditions. The analytical models were developed based on the plastic deformation theory. For general tube bending processes (without the additional tension and pressure), the analytical and FEA predictions agree well with published experimental data. With additional tension and pressure loading, it is found that the analytical and FEA results are in good agreement.

It was seen that internal pressure can alone remove wrinkling and provide a better cross section, but the use of internal pressure alone is limited to the capacity of pressure intensifier. And moreover beyond a certain value of internal pressure the cross section distortion increases. In such cases combination of axial pull and internal pressure can be used. From the parametric study it was seen that with increase in axial pull the rate of decrease in wall thickness was greater at intrados and in the case of axial pull the rate of decrease of wall thickness was greater at extrados. The parametric study conducted

showed that with optimum level of internal pressure and axial pull best results can be obtained.

The contribution of the present work is that the developed analytical models can be used to analyze tooling and process design in the early design stage. This is significant since the commonly used FEA simulation requires extensive part modeling and computation time.

The future work can include improvement in the analytical model by incorporating the effect of the pressure die so a more accurate prediction of wall thickness can be made at the extrados.

REFERENCES

[1] Brewster, K., Sutter, K., Ahmetoglu, M.A., and Altan, T., 1996, "Hydroforming Tube," The Tube and Pipe Quarterly, **7**(4), pp. 34-40.

[2] Denglar, K., 1996, "Exploring Internal High Pressure in Forming of Metal," The Fabricator, **7/8**.

[3] Horton, F., 1997, "Using Forming Simulation in Development of Complex Hydroformed Shapes," *Proceedings of the 2nd annual automotive tube conference*, Dearborn, Michigan, May 13-14, pp.173.

[4] Kim, J., Kang, S.J., and Kang, B.S., 2002, "Computational Approach to Analysis and Design of Hydroforming Process for an Automobile Lower Arm," Computers and Structures, **80,** pp. 1295-1304.

[5] Kervick, R.J., and Springborn, R.K., 1966, *Cold Bending and Forming Tube and Other Sections,* American Society of Tool and Manufacturing Engineers, Dearborn, MI.

[6] Tarana, K., 2002, "Finite Element Simulation of the Tube Hydroforming Process – Bending, Preforming and Hydroforming," Journal of Materials Processing Technology, **127**, pp. 401-408.

[7] Yang, J., Jeon, B., 2001, "The Tube Bending Technology of a Hydroforming Process from an Automotive Part," Journal of Materials Processing Technology, **111**, pp. 175-181.

[8] Miller, J.E., Kyriakides, S., Bastard, A.H., 2001, "On Bend-Stretch Forming of Aluminum Extruded Tubes - I: Experiments," International Journal of Mechanical Sciences, **43**(5), pp. 1283-1317.

[9] Miller, J.E., Kyriakides, S., Bastard, A.H., 2001, "On Bend-Stretch Forming of Aluminum Extruded Tubes - II: Analysis," International Journal of Mechanical Sciences, **43**(5), pp. 1319-1338.

[10] Li, H.Z., Fagerson, R., and Stelson, K.A., 1994, "A Method of Adaptive Control of Rotary-Draw Thin Walled Tube Bending With Spring Back Compensation," *Transactions of the North American Manufacturing Research*, S.M.E, **22**, pp. 25-28.

[11] Brazier, L.G., 1927, "On the Flexure of Thin Cylindrical Shells and Other Sections," Proceedings of the Royal Society of London, **116**, pp. 104-114.

[12] Zang, L.C., and Yu, T.X., 1987, "An Investigation of the Brazier Effect on a Cylindrical Tube Under Pure Elastic-Plastic Bending," International Journal of Pressure Vessel and Piping, **30**, pp.77-86.

[13] Pan, K., and Stelson, K.A., 1995, "On the Plastic Deformation of a Tube During Bending," Journal of Engineering for Industry, **117**, pp. 494-500.

[14] Tang, N.C., 2000, "Plastic-Deformation Analysis in Tube Bending," International Journal of Pressure Vessel and Piping, **77**(12), pp. 751-759.

[15] Corona, E., and Kyriakides, S., 1988, "On the Collapse of Inelastic Tubes Under Combined Bending and Pressure," International Journal of Solids and Structures, **24**, pp. 505-535.

[16] Kyriakides, S., and Ju, G.T., 1992, "Bifurcation and Local Instabilities in Cylinderical Shells Under Bending: Part 1 Experiments," International Journal of Solids and Structures, **29**, pp. 1117-1142.

[17] Corona, E., and Vaze, S.E., 1996, "Buckling of Elastic-Plastic Square Tubes under Bending," International Journal of Mechanical Sciences, **38**(8), pp. 753-775.

[18] Wang, X., Cao, J., 2001, “Wrinkling Limit in Tube Bending,” Journal of Engineering Materials and Technology, **123**(4), pp. 430-435.

[19] Zhan, M., Yang, H., Jiang, Z.Q., Zhao, Z.S., Lin, Y., 2002, “A Study on a 3D FE Simulation Method of the Bending Process of Thin –Walled Tube,” Journal of Materials Processing Technology, **129**, pp. 273-276.

[20] Dyau, J.Y., and Kyriakides, S., (1992), “On the Response of Elastic-Plastic Tubes Under Combined Bending and Tension,” Journal of Offshore Mechanics and Arctic Engineering, **114**, pp.50-62.

[21] Zhu, H., and Stelson, K.A., 2002, “Distortion of Rectangular Tubes in Stretch Bending,” Journal of Manufacturing Science and Engineering, **124**, pp. 886-890.

[22] Duncan J. L., Hu J., and Marciniak Z., *Mechanics of Sheet Metal Forming*, Butterworth-Heinemann, Woburn, MA.

[23] Hosford, W.F., and Caddell, R.M., 1983, *Metal Forming Mechanics and Metallurgy*, Prentice-Hall Inc., Englewood Cliffs, NJ.

[24] LS-DYNA, May 1999, “Keyword User’s Manual,” Livermore Software Technology Corporation, Livermore, CA.

[25] HyperMesh, 2001, “Altair HyperMesh Tutorials Version 5.0,” Altair Engineering Inc., Troy, MI.

[26] Khodayari. G., 2002, “How the Material Influences the Bending for Hydroforming Effects on Ovality, Springback, and Wall Thickness in Tubes,” The Tube and Pipe Journal,

http://www.thefabricator.com/xp/Fabricator/Articles/Tube/Tub02/02web315.xml.

[27] Shr, S.G., 1998, “Bending of Tubes for Hydroforming : a State-of-the-Art Review and Analysis,” M.S. thesis, Ohio State University, Columbus, Ohio

APPENDIX A

SIMULATION OF ROTARY DRAW TUBE BENDING USING LS-DYNA

Finite element analysis consists of three steps Pre-processing, processing and post-processing. HyperMesh was used as pre-processor for the simulation. LS-DYNA was used as the processor while post-processing was done using HyperView.

Preprocessing gives the description about the geometry, material property and boundary conditions. HyperMesh provides different types of collectors to store information; like component collector to store the information about the geometry, material collector to store information about material property and load collector to store information about the loads and boundary conditions. The entire preprocessing has been divided into three steps:

a. Creating collectors

b. Creating geometry

c. Applying boundary condition

d. Applying control cards and data base cards

1 Creating collectors

Four types of collectors are created: material (Mat), property (Prop), component (Comp) and load collector (Load).

1.1 Material collector (*MAT)

The tooling for rotary draw tube bending consists of six parts (five rigid parts and one tube) and hence six material collectors were created. All the collectors are named according to the part. The rigid toolings were specified MAT 20 which is the default rigid material for LD-DYNA. MAT24 (LINEAR _PEICEWISE_PLASTICITY) was used as the material model for the tube. Each material must be assigned material property: - Young's modulus, density, Poisson's ratio. It is essential that units should be consistent because LS-DYNA understands a consistent set of units. The units chosen for simulation are:

Table A-1: Units used in simulation

Mass	Ton
Force	Newton
Pressure	MPa
Time	Second

The material property specified for all the rigid tools are listed in the table 111.The other important thing which needs to be specified is the translational and the rotational constraint of the rigid body.

1.1.1 **Bend die**: It was specified a translation in X and Y direction and rotation about the Z axis.

1.1.2 **Clamp die**: It was specified a translation in X and Y direction and rotation about the Z axis.

1.1.3 **Wiper die**: It was constrained to translate and rotate in all the directions.

1.1.4 **Mandrel**: It was constrained to translate and rotate in all the directions.

1.1.5 **Pressure die**: It has been given translation degree of freedom in X and Y direction and was constrained to rotate in all directions.

1.2 Property collector

Six shell sections were created, one for each part. Each section is assigned to the corresponding material. Shell element, thickness and NIP (number of integration points) were specified for each shell segment.

Four nodded, Belytschko-Tsay shell element with 5 NIP having a thickness of 2.858 mm was specified for the tube.

Four nodded, Belytschko-Tsay shell element with 2 NIP was considered for the rigid parts.

1.3 Component collector

Six component collectors were created and corresponding materials are assigned to each of them.

1.4 Load collector

Two load collectors (bend die rotation and pressure die movement) were created one for the bend die movement and the other one for the pressure die movement. Prescribed Boundary (PRS BOUN) was selected as the load type.

2 Creating Geometry

Here a brief description is provided for modeling al the six parts.

2.1 Bend Die

The bend die consists of two parts: a circular part and a straight part where the clamp die holds the tube. Hence the modeling was done in two steps. The first step was modeling of the circular part and the second step was modeling of the straight part.

2.1.1 **Circular part**

User control torus was used to model the circular part. For this first the nodes were created for selecting the center of the die, major direction and normal direction. Radius and angle of major and minor axis and the element density were specified to get the final model.

2.1.2 **Straight part**

Modeling of the straight part was done using the user controlled cylinder. Nodes were created for selecting the major direction and the center of the cylinder. Radius, angle of the cylinder and the element density was used to complete the modeling.

2.2 Clamp die

Modeling of clamp die was done using user controlled cylinder. Similar to the modeling of the straight portion of the bend die.

2.3 Pressure die

Modeling of clamp die was done using user controlled cylinder. Similar to the modeling of the straight portion of the bend die.

2.4 Wiper die

Modeling of clamp die was done using user controlled cylinder, similar to the modeling of the straight portion of the bend die.

2.5 Mandrel

A plug mandrel is used for the simulation. The modeling procedure for the mandrel is same as the clamp die .The only difference is that instead of span angle of 180^{o} , span angle of 360^{o} is specified.

2.6 Tube

Modeling of clamp die was done using user controlled cylinder similar to the modeling of the mandrel.

3 Boundary Condition

After the modeling is completed Boundary condition is applied to the parts.

3.1 Contact

For defining the contact between different surface pair's two different types of contact algorithm are chosen

3.1.1 Contact_surface_to_surface

This is used to define the surface contact between tube-bend die, tube–pressure die, tube–wiper die, and tube–mandrel. Contact option is specified by selecting master surface and the slave surface. The rigid body is always selected as the master surface and the blank (which is finely meshed) is always selected as the slave surface.

The coefficient of static and dynamic friction between the Tube-bend-die is specified as 0.10 and the coefficient of static friction between the tube-pressure die, tube-wiper die, tube –mandrel is specified as 0.5

3.1.2 Constrained_extra_nodes_set

A node set is made of all the nodes of the tube towards the clamp side and they are added to the nodes of the clamp hence making an ideal Clamp die.

3.2 Pressure

A pressure of 50 MPa is applied to the pressure die for which elements of pressure die are selected. In a shell element, pressure always acts in the direction of the normal, so a negative value of magnitude must be specified to change the direction of pressure.

Internal pressure in the tube is also specified in the same way.

3.3 Checking Penetration

Penetration check is done so as to check if the master segment would penetrate in the slave segment during the simulation. To avoid penetration two things have to be kept in mind:

The normal should be opposite to each other.If both the normal point towards each other then normal of one of the surface should be reversed.

The slave surface (tube) should have a finer mesh than the master surface (rigid part). If there is a penetration then the element size of the tube needs to be decreased.

3.4 Displacement Boundary condition

3.4.1 Bend die

Rotation about Z axis and the load curve are specified The load curve is a curve between the time and angle (in radians)

3.4.2 Pressure die

Translation in X axis and the load curve are specified. The load curve is a curve between the time and displacement (in mm)

APPENDIX B

INPUT DECK FOR ROTARY DRAW TUBE BENDING

```
*KEYWORD
$$      Units Ton, N, MPa, sec
$$
*CONTROL_TERMINATION
$$  ENDTIM    ENDCYC     DTMIN    ENDENG    ENDMAS
   0.0365         0       0.0       0.0       0.0
*CONTROL_SHELL
$$  WRPANG    ITRIST     IRNXX    ISTUPD    THEORY       BWC     MITER      PROJ
     20.0         2         0         1         2         2         1         0
*CONTROL_HOURGLASS
$$     IHQ        QH
       2       0.1
*CONTROL_BULK_VISCOSITY
$$      Q2        Q1
      1.5      0.06
*CONTROL_DAMPING
     250       .001      .995
*CONTROL_CONTACT
$$  SLSFAC    RWPNAL    ISLCHK    SHLTHK    PENOPT    THKCHG     ORIEN
      0.1       1.0         2         2         1         1         1
$$  URSTR    USRFRC     NSBCS    INTERM     XPENE     SSTHK      ECDT   TIEDPRJ
       0         0        10         0       4.0         1         0         0
     0.0       0.0       0.0       0.0       0.0       0.0       0.0
*CONTROL_OUTPUT
$$   NPOPT    NEECHO    NREFUP    IACCOP     OPIFS    IPNINT    IKEDIT
       1         3         1         0       0.0         0       100         0
*CONTROL_ENERGY
$$    HGEN      RWEN    SLNTEN     RYLEN
       2         2         2         2
$$
$$DATABASE_OPTON… Control Cards for ASCII output
$$
$$
*DATABASE_GLSTAT
1.0000E-04
*DATABASE_BINARY_D3PLOT
$$ DT/CYCL      LCDT      BEAM      NPLTC
3.0000E-03         0         0         0
*DATABASE_BINARY_D3THDT
$$ DT/CYCL      LCID
      0.0         0
*DATABASE_EXTENT_BINARY
$$   NEIPH     NEIPS    MAXINT    STRFLG    SIGFLG    EPSFLG    RLTFLG    ENGFLG
       0         0         3         0         1         1         1         1
$$  CMPFLG    IEVERP    BEAMIP     DCOMP      SHGE     STSSZ
       0         0         0         1         1         1
$$
$$MATERIAL PROPERTIES
$$
*MAT_RIGID
$HMNAME MATS       1matrigid
```

```
       17.8300E-09  207000.0       0.3       0.0       0.0       0.0
      1.0         0         0
      0.0       0.0       0.0       0.0       0.0       0.0
*MAT_RIGID
$HMNAME MATS       3matrigid.1
       37.8300E-09  207000.0       0.3       0.0       0.0       0.0
      1.0         7         4
      0.0       0.0       0.0       0.0       0.0       0.0
*MAT_RIGID
$HMNAME MATS       4matrigid.2
       47.8300E-09  207000.0       0.3       0.0       0.0       0.0
      1.0         7         7
      0.0       0.0       0.0       0.0       0.0       0.0
*MAT_RIGID
$HMNAME MATS       5matrigid.3
       57.8300E-09  207000.0       0.3       0.0       0.0       0.0
      1.0         6         7
      0.0       0.0       0.0       0.0       0.0       0.0
*MAT_PIECEWISE_LINEAR_PLASTICITY
$HMNAME MATS       2MAT24_2
       28.9000E-09  210000.0       0.3     210.0     900.0       0.0
      0.0       0.0                 0         0
$$ HM Entries in Stress-Strain Curve =         8
      0.0     0.000       0.0       0.0       0.0       0.0       0.0
      0.0       0.0       0.0       0.0       0.0       0.0       0.0
$$
$$PART PROPERTIES
$$
*PART_INERTIA
$HMNAME COMPS       1die     0       0
$HMCOLOR COMPS       1       7

       1         1         3         0         0         0         0
    100.0     100.0       0.07.6500E-05         0
     9.82      5.49-2.500E-04      16.62.8900E-04      24.3
      0.0       0.0       0.0       0.0       0.0       0.0
*CONSTRAINED_RIGID_BODIES
       1         9
       1        11
*CONSTRAINED_EXTRA_NODES_SET
       9         3
*PART
$HMNAME COMPS       2tube
$HMCOLOR COMPS       2       6

       2         2         2         0         0         0         0
*PART
$HMNAME COMPS       4pressure
$HMCOLOR COMPS       4       7

       4         1         5         0         0         0         0
*PART
$HMNAME COMPS       7wiper
$HMCOLOR COMPS       7       6

       7         1         4         0         0         0         0
```

```
*PART
$HMNAME COMPS       9clamp
$HMCOLOR COMPS       9       3

       9        1        1        0        0        0        0
*PART
$HMNAME COMPS      11diepart
$HMCOLOR COMPS      11       7

      11        1        1        0        0        0        0
$$
$$SECTION PROPERTIES
$$
*SECTION_SHELL
$HMNAME PROPS       1shell section
       1        2      1.0        5      0.0      0.0        0
    7.01     7.01     7.01     7.01      0.0
$HMNAME PROPS       2shell-tube
       2        2      1.0        5      0.0      0.0        0
   2.858    2.858    2.858    2.858      0.0
$$
$$BOUNDARY CONDITION
$$
*BOUNDARY_PRESCRIBED_MOTION_RIGID
$HMNAME LOADCOLS       1boundary
$HMCOLOR LOADCOLS       1       7
       1        7        2        1     -1.0        01.0000E+28       0.0
*BOUNDARY_PRESCRIBED_MOTION_RIGID
$HMNAME LOADCOLS       2PrescribedMtnRgd 2
$HMCOLOR LOADCOLS       2       1
       4        2        2        3     -1.0        01.0000E+28
*CONTACT_SURFACE_TO_SURFACE
$HMNAME GROUPS       4contact-tube-prseeure
$HMCOLOR GROUPS       4       1
       2       11        3        3                         0
    0.05     0.05      0.0      0.0     20.0        1
     1.0      1.0      0.0      0.0      1.0      1.0      1.0
*CONTACT_SURFACE_TO_SURFACE
$HMNAME GROUPS       5contact-tube-wiper
$HMCOLOR GROUPS       5       1
       2        4        3        3                         0
    0.05     0.05      0.0      0.0     20.0        1      0.0      0.0
     1.0      1.0      0.0      0.0      1.0      1.0      1.0      1.0
*CONTACT_SURFACE_TO_SURFACE
$HMNAME GROUPS       7tube-die
$HMCOLOR GROUPS       7       1
       2        1        3        3                         0
    0.10     0.10      0.0      0.0      0.0        1
     1.0      1.0      0.0      0.0      1.0      1.0      1.0
*CONTACT_SURFACE_TO_SURFACE
       2        9        3        3
     0.1      0.1      0.0      0.0      0.0        1
     1.0
$$
$$VECTORS AND CURVE
$$
```

```
*DEFINE_VECTOR
$HMNAME VECTORCOL       1auto1
$HMCOLOR VECTORCOL       1       1
       1     100.0     100.0       0.0     100.0     100.0     -10.0
*DEFINE_CURVE
$HMNAME CURVES       1curve1
$HMCOLOR CURVES       1       1
$HMCURVE     1    1 curve1
       1         0       1.0       1.0       0.0       0.0         0
             0.0               0.0
3.00000000000000E-03             0.1309
6.00000000000000E-03           0.261799
             0.009           0.392699
             0.012            .522599
             0.015            .654498
             0.018            .785398
             0.021            .916298
             0.024           1.047198
             0.027           1.178098
             0.030           1.308997
             0.033           1.439897
             0.036           1.570796
            0.0365           1.701696
*DEFINE_CURVE
$HMNAME CURVES       4curve1.1
$HMCOLOR CURVES       4       1
$HMCURVE     1    1 curve1       tube
       2         0       1.0       1.0       0.0       0.0         0
             0.0               5.0
          0.0365               5.0
*DEFINE_CURVE
$HMNAME CURVES       2curve2
$HMCOLOR CURVES       2       1
$HMCURVE     1    1 curve2
       3         0       1.0       1.0       0.0       0.0         0
             0.0               0.0
3.00000000000000E-03              10.0
             0.011              15.0
             0.020              20.0
           0.0365              25.0
*DEFINE_CURVE
$HMNAME CURVES       4curve1.1
$HMCOLOR CURVES       4       1
$HMCURVE     1    1 curve1       Pressure
       4         0       1.0       1.0       0.0       0.0         0
             0.0              50.0
          0.0365              50.0
*DEFINE_CURVE
       5         0       1.0       1.0       0.0       0.0         0
             0.0               0.0
             0.001             300.0
             0.045             300.0
*NODE
       4         239.04          100.0           32.2
       5 238.76563632066 108.73039383535           32.2
       6 237.94362807076 117.42633279478           32.2
```

```
      7 236.57721934131 126.05349797999          32.2
      8 234.67180272332  134.5778419114          32.2
      9 232.23489802567 142.96572289789          32.2
     10  229.2761225979 151.18403780527          32.2
     11 225.80715337487  159.2003526992          32.2
     12 221.84168079329  166.9830308471          32.2
    ..
    ..
  16541 212.99138814707 173.64545454545 -18.92907341988
  16542 208.42550134103 184.03636363636 -9.979602790705
  16543 212.99138814707 184.03636363636 -18.92907341988
  *ELEMENT_SHELL
     58      1    189    187    188    188
     62      1    200    199    201    201
    113      1    233    228    229    229
    184      1    272    273    292    292
    201      1    309    242    310    310
    221      1    122    323    123    123
    246      1    330    336    329    329
    ..
    ..
  14907     11   15533   15534   15540   15538
  14908     11   15538   15540   15539   15537
$$
$$ NODE SETS
$$
*SET_NODE_LIST
$HMSET
$NODES OF TUBE CONSTRAINED TO CLAMP
       3      0.0      0.0      0.0      0.0
    9760     9761     9762     9763     9764     9765     9766     9767
    9768     9769     9770     9771     9772     9773     9774     9775
    9776     9777     9778     9779     9780     9781     9782     9783
    9784     9785     9786     9787     9788     9789     9790     9791
    9792     9793     9794     9795     9796     9797     9798     9799
    9800     9801     9802     9803     9804     9805     9806     9807
    9808     9809     9810     9811     9812     9813     9814     9815
     ..
     ..
   11283    11284    11285    11286    11287    11288    11289    11290
   11291    11292    11293    11294    11295    11296    11297    11298
   11299    11300    11301    11302    11303    11304    11305    11306
   11307    11308    11309    11310    11311    11312    11313    11314
*SET_NODE_LIST
$HMSET
$NODES TO WHICH AXIAL PULL IS APPLIED
       4      0.0      0.0      0.0      0.0
    9928     9929     9930     9931     9932     9933     9934     9935
    9936     9937     9938     9939     9940     9941     9942     9943
    9944     9945     9946     9947     9948     9949     9950     9951
    9952     9953     9954     9955     9956     9957     9958     9959
    9960     9961     9962     9963     9964     9965     9966     9967
    9968     9969     9970
$$
$$LOAD APPLIED
$$
```

```
*LOAD_SEGMENT
$$ HMNAME LOADCOLS       2PrescribedMtnRgd 2
$$ PRESSURE APPLIED TO PRESSURE DIE
       4     -1.0      0.0     16037     16036     16041     16040
       4     -1.0      0.0     16036     16024     16023     16041
       4     -1.0      0.0     16040     16041     16016     16015
       4     -1.0      0.0     16041     16023     16017     16016
       4     -1.0      0.0     16038     16037     16040     16042
       4     -1.0      0.0     16042     16040     16015     16014
       4     -1.0      0.0     16001     16039     16043     16002
       ..
       ..
       4     -1.0      0.0     16410     16318     16319     16408
       4     -1.0      0.0     16369     16370     16411     16395
       4     -1.0      0.0     16370     16371     16410     16411
       4     -1.0      0.0     16395     16411     16409     16394
       4     -1.0      0.0     16411     16410     16408     16409
*LOAD_SEGMENT
$$ HMNAME LOADCOLS       2PrescribedMtnRgd 2
$$ INTERNAL PRESSURE APPLIED TO TUBE
       2     -1.0      0.0     10847     10852     10848     10846
       2     -1.0      0.0     10827     10826     10852     10847
       2     -1.0      0.0     10729     10728     10850     10851
       2     -1.0      0.0      9825     10729     10851      9826
       2     -1.0      0.0     10851     10850     10848     10849
       2     -1.0      0.0      9826     10851     10849      9827
       2     -1.0      0.0     10845     10850     10728     10727
       2     -1.0      0.0     10846     10848     10850     10845
      ..
      ..
       2     -1.0      0.0     15113     15177     15173     15114
       2     -1.0      0.0     15166     15178     15147     15146
       2     -1.0      0.0     15178     15177     15148     15147
       2     -1.0      0.0     15165     15174     15178     15166
       2     -1.0      0.0     15174     15173     15177     15178
*LOAD_NODE_SET
$HMNAME LOADCOLS       2PrescribedMtnRgd 2
$HMCOLOR LOADCOLS       2       1
       4       2       5      1.0
*END
```

VITA

Rohit Agarwal

HIG 79 Sector E

Aliganj, Lucknow, India

August 12, 1979.....Born, Kanpur, U.P., India

2001 – 2004.....M.S. Mechanical Engineering,
Texas A&M University, USA

1996 - 2000.....B.E. Mechanical Engineering,
Bangalore University, India

Email address: rohitagarwal@tamu.edu